

1 **EBV miRNAs are potent effectors of tumor cell transcriptome remodeling in promoting immune  
2 escape.**

3

4

5 Nathan Ungerleider<sup>1</sup>, Whitney Bullard<sup>3</sup>, Mehmet Kara<sup>4</sup>, Xia Wang<sup>1</sup>, Claire Roberts<sup>1</sup>, Rolf Renne<sup>2</sup>, Scott  
6 Tibbetts<sup>\*2</sup>, Erik Flemington<sup>\*1</sup>

7

8

9 <sup>1</sup> Department of Pathology, Tulane University School of Medicine, Tulane Cancer Center, New Orleans, LA  
10 70112, United States of America

11 <sup>2</sup> Dept. of Molecular Genetics and Microbiology, UF Health Cancer Center, University of Florida, Gaines-  
12 ville, Florida, United States of America

13

14

15 \* To whom correspondence should be addressed.

16 Erik Flemington, Tel: 504-988-1167; Email: erik@tulane.edu

17

18 \* Correspondence may also be addressed to:

19 Scott Tibbetts, Tel: 352-273-5628; Email: stibbe@ufl.edu

20

21

22 **ABSTRACT**

23

24 Epstein Barr virus (EBV) contributes to the tumor phenotype through a limited set of primarily non-coding  
25 viral RNAs, including 31 mature miRNAs. Here we investigated the impact of EBV miRNAs on remodeling  
26 the tumor cell transcriptome. Strikingly, EBV miRNAs displayed exceptionally abundant expression in pri-  
27 mary EBV-associated Burkitt's Lymphomas (BLs) and Gastric Carcinomas (GCs). To investigate viral  
28 miRNA targeting, we used the high-resolution approach, CLASH in GC and a BL cell models. Affinity con-  
29 stant calculations of targeting efficacies for CLASH hits showed that viral miRNAs bind their targets more  
30 effectively than their host counterparts, as did Kaposi's sarcoma-associated herpesvirus (KSHV) and mu-  
31 rine gammaherpesvirus 68 (MHV68) miRNAs. Using public BL and GC RNA-seq datasets, we found that  
32 high EBV miRNA targeting efficacies translates to enhanced reduction of target expression. Pathway anal-  
33 ysis of high efficacy EBV miRNA targets showed enrichment for innate and adaptive immune responses.  
34 Inhibition of the immune response by EBV miRNAs was functionally validated *in vivo* through the finding of  
35 inverse correlations between EBV miRNAs and immune cell infiltration and T-cell diversity in TCGA GC  
36 dataset. Together, this study demonstrates that EBV miRNAs are potent effectors of the tumor transcrip-  
37 tome that play a role in suppressing the host immune response.

38

39 **AUTHOR SUMMARY**

40

41 Burkitt's Lymphoma and gastric cancer are both associated with EBV, a prolific DNA tumor virus that la-  
42 tently resides in nearly all human beings. Despite mostly restricting viral gene expression to noncoding  
43 RNAs, EBV has important influences on the fitness of infected tumor cells. Here, we show that the miRNA  
44 class of viral noncoding RNAs are a major viral contributor to remodeling the tumor cell regulatory ma-  
45 chinery in patient tumor samples. First, an assessment of miRNA expression in clinical tumor samples  
46 showed that EBV miRNAs are expressed at unexpectedly high levels relative to cell miRNAs. Using a  
47 highly specific miRNA target identification approach, CLASH, we comprehensively identified both viral  
48 and cellular microRNA targets and the relative abundance of each microRNA-mRNA interaction. We also  
49 show that viral microRNAs bind to and alter the expression of their mRNA targets more effectively than  
50 their cellular microRNA counterparts. Pathway analysis of the most effectively targeted mRNAs revealed  
51 enrichment of immune signaling pathways and we show a corresponding inverse correlation between EBV  
52 miRNA expression and infiltrating immune cells in EBV positive primary tumors. Altogether, this study  
53 shows that EBV miRNAs are key regulators of the tumor cell phenotype and the immune cell microenvi-  
54 ronment.

55

56 **INTRODUCTION**

57

58 The Epstein Barr Virus (EBV) is a ubiquitous gammaherpesvirus ( $\gamma$ HV) that establishes lifelong infections  
59 in over 90% of the world's population. Since its discovery as the major etiological agent of endemic  
60 Burkitt's lymphoma (BL)(1), EBV has been causally associated with other malignancies including NK/T cell  
61 lymphoma(2), diffuse large B cell lymphoma(3), Hodgkin's lymphoma(4), nasopharyngeal carcinoma(5)  
62 and gastric carcinoma (GC)(6). Arising from infected founder cells, these tumors maintain a dependence  
63 on the virus as they progress(7).

64  $\gamma$ HVs utilize two distinct strategies, referred to as lytic and latent replication, to expand the infected  
65 host cell population(8). The lytic replication program is a process utilized by all viruses to replicate and  
66 package their genetic content for spread through cell-to-cell transfer. This strategy produces a large  
67 number of virions but it destroys the host cell and triggers a strong local immune response(9). The viral  
68 latency program, the phase most closely linked with cancer, is associated with the expression of a small  
69 number of genes that support the growth and health of the infected cell(10-16) and by extension, the  
70 growth and health of its viral occupant. In this phase of the virus infection cycle, viral and host genomes  
71 are replicated concordantly and distributed to daughter cells(17), resulting in an expansion of the infected  
72 cell population that is independent of virion production. This form of intracellular replication minimizes  
73 immune reactivity, allowing the virus to discretely double the pool of infected cells at each mitotic cycle.

74 In EBV-associated BLs and GCs, the latency gene expression program is especially restrictive,  
75 with the only ubiquitous and consistently expressed viral protein being the replicative factor, EBNA1(18).  
76 More abundantly expressed are a group of viral noncoding RNAs that allow the virus to modulate the host  
77 cell environment without eliciting a strong adaptive immune response. These include two short noncoding  
78 RNAs (EBER1 and EBER2)(19), a long noncoding RNA (RPMS1)(20), circular RNAs(21, 22), and the viral  
79 miRNAs(23).

80 MiRNAs function by targeting complementary mRNAs for destruction(24). By interacting with an  
81 average of 90 unique transcripts(25), a single miRNA can have a substantial impact on the cellular  
82 transcriptome(26-30). The genomes of EBV, KSHV, and MHV68 potentially encode 44, 25, and 28

83 miRNAs(31-34), theoretically endowing these viruses with the capacity to control nearly every pathway in  
84 the cell. Several previous studies have used broad-scale approaches such as AGO-CLIP to uncover viral  
85 miRNA targets(35-37), and some of these miRNA-target interactions have since been shown to interrupt  
86 apoptosis(38), prevent reactivation(39), and block interferon signaling(40). The AGO-CLIP approach,  
87 however, requires bioinformatic inferences to determine miRNA-mRNA pairings, precluding analysis of  
88 binding efficacy and limiting detection to canonical interactions. Here we used a modified version of a  
89 more comprehensive and quantitative approach, Crosslinking, Ligation, and Sequencing of Hybrids  
90 (CLASH)(41), called qCLASH(42), to broadly uncover *bona fide* targets of EBV miRNAs. Through  
91 integration of mRNA, miRNA, and hybrid abundances, we examine the global binding properties and  
92 targeting efficacies inherent to  $\gamma$ HV miRNAs. Assessing pathway enrichment of the highest targeting  
93 efficacy EBV miRNA-target interactions shows enrichment for innate and adaptive immune responses.  
94 Utilizing clinical BL and GC datasets, we explore the roles of EBV miRNAs in primary tumors and  
95 demonstrate a role for EBV miRNAs in dampening the immune response to viral infection and  
96 oncogenesis.

97

## 98 MATERIALS AND METHODS

99

### 100 Cell culture

101 Akata (obtained from Kenzo Takada) and SNU719 (Korean Cell Line Bank) cells were grown in RPMI  
102 1640 media (ThermoFisher Scientific, catalog no. SH30027) supplemented with 10% fetal bovine serum  
103 (FBS; ThermoFisher Scientific, catalog no. 10437), and incubated at 37°C in 5% CO<sub>2</sub>.

104

### 105 Clinical data

106 Aligned RNA and miRNA sequencing reads, deposited by the BGLSP and TCGA, were downloaded from  
107 the Genomic Data Commons (GDC)(43). RNA sequencing alignments were converted to FASTQ format  
108 using the following command:

109 `samtools sort -@ 19 -n $bamfile | samtools fastq -@ 19 -1 $fq1 -2 $fq2 -0 /dev/null -s /dev/null -n -F 0x900`

110 –

111

112 The resulting raw sequencing reads were pseudoaligned to the human (GENCODE GRCh38.p13)(44) and  
113 EBV(45) transcriptomes using kallisto v0.46.0(46) (including the “-rf-stranded” flag for BL sequencing  
114 reads, which were strand-specific). The underlying counts or transcripts per million (t.p.m.) values were  
115 summed and assigned to each gene. BL analysis was restricted to the “Discovery” cohort due to the re-  
116 ported higher RNA sequencing quality of these samples(47). With the exception of *Figure S1*, GC analysis  
117 was restricted to microsatellite stable samples(48).

118

119 Aligned miRNA sequencing reads were converted to FASTQ format using the following command:  
120 *samtools fastq -F 0x900 \$bamfile*

121

122 Raw miRNA sequencing reads were aligned to an index of mature human and EBV miRNA sequences  
123 (miRbase v22) via bowtie with the following command:

124 *bowtie \$mir\_index -n 3 -m 10 --best --strata -p 10 -S \$mir\_fastq*

125

## 126 **UV Crosslinking**

127 qCLASH was performed as previously described<sup>1</sup>, with 3 biological replicates processed for each cell line.  
128 SNU719 cells were trypsinized, resuspended in RPMI 1640 plus 10% FBS, then washed twice with PBS.  
129 Akata cells were washed twice with PBS. Both cell lines were resuspended in 10 mL PBS then crosslinked  
130 with 250 nm  $\lambda$  UV light for a total exposure of 600J/cm<sup>2</sup>. 50 million cells were transferred to a 1.5 mL tube,  
131 pelleted at 800 x g for 5 minutes, and stored at -80°C before processing as described below.

132

## 133 **Cell lysis**

134 Cell pellets were thawed and resuspended in 500  $\mu$ l cell lysis buffer (50 mM HEPES (pH 7.5), 150 mM  
135 KCl, 2mM EDTA, 1mM NaF, 0.5% NP-40, 0.5 mM DTT, and 1x protease inhibitor cocktail (Roche, catalog  
136 no. 11836170001)). Cells were lysed for 15 minutes on ice then treated with 10  $\mu$ L of RQ1 DNase  
137 (Promega, catalog no. M610A) for 5 minutes at 37°C, while shaking at 1,000 rpm. Lysates were cleared by

138 a 21,000 x g centrifugation for 15 minutes at 4°C. Supernatants were treated for 15 minutes with 0.5  $\mu$ L  
139 RNase T1 (ThermoFisher Scientific, catalog no. EN054) at 22°C.

140

141

142 **Preparation of Protein G beads**

143 6 mg of Protein G Dynabeads (Invitrogen, catalog no. 1004D) were washed 3 times then resuspended in  
144 PBST (pH 7.2). A final concentration of 200ug/ml of AffiniPure rabbit  $\alpha$ -mouse IgG (Jackson Immu-  
145 noResearch, catalog no. 315-005-008) was added and beads were incubated on a rotator for 50 minutes  
146 at 25°C. The complexes were washed 3 times with PBST (5 minutes each), then resuspended in 1 mL of  
147 PBST. 10  $\mu$ g of pan-AGO antibody (gift from Zissimos Mourelatos) was added and samples were rotated  
148 for 16 hours at 4°C. Beads were then washed 4 times with wash buffer (1x PBS, 0.1% SDS, 0.5% sodium  
149 deoxycholate, and 0.5% NP-40).

150

151 **Immunoprecipitation**

152 1 mL of crosslinked cell lysate was added to the pelleted  $\alpha$ -AGO beads. Tubes were put on a rotator and  
153 incubated for 16 hours at 4°C. The bead complexes were then centrifuged and washed 3 times with cell  
154 lysis buffer, followed by 4 times each with 1x PXL (1x PBS, 0.1% SDS, 0.5% sodium deoxycholate, 0.5%  
155 NP-40), 5x PXL (5x PBS, 0.1% SDS, 0.5% sodium deoxycholate, 0.5% NP-40), high-stringency wash  
156 buffer (15 mM Tris-HCl (pH 7.5), 5 mM EDTA, 2.5 mM EGTA, 1% Triton X-100, 1% sodium deoxycholate,  
157 0.1% SDS, 120 mM NaCl, 25 mM KCl), high salt wash buffer (15 mM Tris-HCl (pH 7.5), 5 mM EDTA, 2.5  
158 mM EGTA, 1% Triton X-100, 1% sodium deoxycholate, 0.1% SDS, 1 M NaCl), then polynucleotide kinase  
159 (PNK) buffer (50 mM Tris-HCl (pH 7.5), 10 mM MgCl<sub>2</sub>, 0.5% NP-40).

160

161 **Ligation of RNA ends**

162 RNA 5'-ends were phosphorylated using 4  $\mu$ l T4 PNK (NEB, catalog no. M0201) in a solution consisting of  
163 8  $\mu$ l 10x PNK buffer, 2  $\mu$ l RNasin Plus (Promega, catalog no. N2615), 0.8  $\mu$ l 100 mM ATP (ThermoFisher  
164 Scientific, catalog no. R0041), and 65.2  $\mu$ l ddH<sub>2</sub>O. Bead complexes were incubated for 40 minutes at 10°C  
165 then washed 3 times in PNK buffer. RNAs were then ligated by rotating for 16 hours at 4°C in 500  $\mu$ l of

166 RNA ligation solution (50  $\mu$ l 10x T4 RNA ligase buffer, 60  $\mu$ l 50% polyethylene glycol 8000, 125  $\mu$ l 4M KCl,  
167 12.5  $\mu$ l RNasin Plus, 5  $\mu$ l 100 mM ATP, 321.25  $\mu$ l ddH<sub>2</sub>O, and 50  $\mu$ l T4 RNA ligase 1 (NEB, catalog no.  
168 M0204). Bead complexes were then washed 3 times with 1 mL PNK buffer. Next, 80  $\mu$ l of dephosphoryla-  
169 tion solution (8  $\mu$ l 10x dephosphorylation buffer, 2  $\mu$ l RNasin Plus, 67  $\mu$ l ddH<sub>2</sub>O, and 3  $\mu$ l alkaline phos-  
170 phatase (Roche, catalog no. 10713023001)) was added to the beads, and RNA dephosphorylation was  
171 achieved by incubating samples for 40 minutes at 10°C, with intermittent 1,000 rpm shaking every 2  
172 minutes for 15 seconds. The bead complexes were washed 2 times with 1 mL EGTA buffer (50 mM Tris-  
173 HCl (pH 7.5), 20 mM EGTA, 0.5% NP-40), and then three times with 1 mL PNK buffer.

174

### 175 **Ligation of 3'-adapter**

176 To ligate the miRCat-33 3'-linker (5'-TGGAAATTCTCGGGTGCCAAGG-3') to the newly formed RNA hy-  
177 brids, beads were incubated with 42  $\mu$ l ddH<sub>2</sub>O, 8  $\mu$ l 10 $\times$  T4 RNA ligase buffer, 16  $\mu$ l 50% PEG-8000, 2  $\mu$ l  
178 RNasin Plus, 8 pM of linker, and 4  $\mu$ l T4 RNA ligase 2 (NEB, catalog no. M0239) for 16 hours at 16°C, with  
179 1,000 rpm shaking every 2 minutes for 15 seconds. Bead complexes were then washed 3 times in PNK  
180 buffer.

181

### 182 **Elution and RNA extraction**

183 Bead complexes were incubated in 100  $\mu$ l of elution buffer (100 mM NaHCO<sub>3</sub>, 1% SDS) for 15 minutes at  
184 25°C on a 1,400 rpm shaker. After spinning at 1,000g for 1 minute, the elution buffer was transferred to a  
185 new tube. An additional 100  $\mu$ l of elution buffer was added to the bead complexes, elution was repeated  
186 and the eluates were then combined. To improve RNA phase separation of crosslinked RNA-AGO com-  
187 plexes, proteins were digested using proteinase K. 10  $\mu$ l of proteinase K (Roche, catalog no.  
188 03115887001) in 40  $\mu$ l of proteinase K buffer (100 mM Tris-HCl (pH 7.5), 50 mM NaCl, 10 mM EDTA )  
189 was added to the 200  $\mu$ l of eluate and samples were incubated at 37°C for 20 min. Samples were then  
190 subjected to phenol-chloroform extraction to purify the RNA.

191

### 192 **CLASH library preparation**

193 RNA ends were phosphorylated, followed by ligation of the Solexa 5' linker (invddT-GTTCArGrAr-  
194 GrUrUrCrUrArCrArGrUrCrCrGrArCrUrC-OH ). RNA was re-extracted via phenol-chloroform, as de-  
195 scribed above. Sequencing libraries were prepared using the Illumina TruSeq Small RNA Sample Prep kit  
196 according to manufacturer's instructions, and cDNA was generated using SuperScript III reverse transcrip-  
197 tase (Invitrogen, catalog no. 18080093). The resulting samples were sequenced on an Illumina HiSeq  
198 2500 machine.

199

200 **RNA sequencing**

201 RNA was extracted from Akata and SNU719 cells using TRIzol (ThermoFisher Scientific, catalog no.  
202 15596026). Extraction was performed according to the manufacturer's instructions with one additional step  
203 included to improve the purity of the RNA: following isopropanol precipitation, RNA was reconstituted in  
204 200  $\mu$ l ddH<sub>2</sub>O with 20  $\mu$ l 3M sodium acetate and 500  $\mu$ l ethanol, stored at -20°C for 16 hours, spun down  
205 at 20,000 x g for 30 minutes at 4°C, and then resuming the manufacturers protocol with the 70% ethanol  
206 wash step. Small fraction sequencing libraries were prepared using the Illumina TruSeq Small RNA Li-  
207 brary Prep Kit (Illumina, catalog no. RS-200-0012), and poly-A sequencing libraries (HE2.1 and TIVE  
208 cells) were generated using the TruSeq RNA Sample Prep Kit (Illumina, catalog no. FC-122-1001).

209

210 **Bioinformatic analysis**

211 Adapter sequences were removed from raw sequencing reads using Trimmomatic<sup>2</sup>. A transcriptome index  
212 was generated for bowtie2<sup>3</sup> alignment, as previously described<sup>4</sup>, with the following modifications: a.  
213 GRCh38 transcript sequences were used (obtained from Gencode<sup>5</sup>; version 33), b. Annotated viral tran-  
214 scripts<sup>6</sup> and miRNA sequences (obtained from mirBase<sup>7</sup>) were included in the index. Processed reads  
215 were aligned to the human and viral transcriptome indexes using bowtie2 v2.3.3; alignments run with the  
216 following parameters: -D 20 -R 3 -N 0 -L 16 -k 20 --local -i S,1,0.50 --score-min L,18,0 --ma 1 --np 0 --mp  
217 2,2 --rdg 5,1 --rfg 5,1). Hybrid alignments were retrieved from aligned reads using the *hyb* pipeline<sup>8</sup>  
218 (<https://github.com/gkudla/hyb>). The structure and binding energies of each hybrid was predicted using the  
219 *RNAcofold* algorithm of the *Vienna RNA* package<sup>9</sup>.

220

221 **Targeting efficacy**

222 Targeting efficacy for each miRNA-mRNA hybrid was calculated using the following equation:

223 
$$t_{(microRNA_x, mRNA_y)} = \frac{microRNA_x:mRNA_y \text{ (h.c.p.m.)}}{microRNA_x \text{ (c.p.m.)} \times mRNA_y \text{ (t.p.m.)}}$$

224 
$$miRNA:mRNA \text{ hybrid counts per million (h.c.p.m.)} = 10^6 \times \left( \frac{microRNA_x:mRNA_y \text{ counts}}{\sum microRNA_n:mRNA_n \text{ counts}} \right)$$

225 Hybrid counts were obtained via CLASH, mRNA t.p.m. were obtained from RNA-sequencing, and *miRNA*  
226 *c.p.m.* levels were quantified via small fraction sequencing.

227

228 **Principal component analysis**

229 BL gene expression counts were transformed using the *normTransform* function of the *DESeq2* R pack-  
230 age(49). GC gene expression counts were transformed using the *vsd* function of the *vsn* R package(50).  
231 Transformed counts were ranked by variance, and PCA was applied to the top 500 most variable genes in  
232 each tumor type using the *plotPCA* function of *DESeq2*. Each of the resulting principal components were  
233 compared to each relevant clinical covariate via logistic regression. *Pseudo-R<sup>2</sup>* values(51) were calculated  
234 for each principal component and covariate pair using the *PseudoR2* of the *desctools* R package.

235

236 **Pathway analysis**

237 CLASH derived mRNA targets for each virus and corresponding host were ranked by targeting efficacy in  
238 each cell line. Protein-protein interaction (PPI) and expression correlation networks were assembled for  
239 each of the top 20 targets using STRING(52) with default parameters, limited to 20 direct and 10 additional  
240 node proteins per queried “seed” gene. The resulting genes were explored for pathway enrichment with  
241 the *enrichR*(53) API, interrogating the Reactome library of pathways. Pathway enrichment was considered  
242 significant if the adjusted P-value < 0.05. All significant pathways were assigned to each seed gene.

243

244 **RESULTS**

245

246 **High expression of viral miRNAs in EBV-associated tumors**

247 BLs and GCs are aggressive tumors with distinct etiologies. Pediatric BL is a B-cell malignancy endemic  
248 to sub-Saharan Africa(47) that is characterized by the t(8;14)(q24;q32) *MYC:IGH* translocation(54, 55).  
249 GCs encompass a diverse group of epithelial tumors(56) originating from the stomach lining that have a  
250 broader epidemiology(57). Despite overt differences in pathology and etiology, nearly all endemic BLs  
251 (over 90%)(47) and a subset of GCs (~10%)(6) are causally infected with EBV. As a first assessment of  
252 the viral contributions to these tumors, we performed principle component analysis (PCA) of 86 BL(47) (66  
253 EBV+) and 235 GC(58) (24 EBV+) cell transcriptomes. Applying logistic regression to each of the top 10  
254 (BL) or 15 (GC) principal components revealed that EBV status is a major distinguishing clinical covariate  
255 in both tumor types (*Figure 1A; Figure S1*), indicating that EBV is likely a key determinant in shaping the  
256 tumor transcriptome.

257 To investigate underlying features of EBV that contribute to the tumor phenotype, we first carried  
258 out a quantitative assessment of the viral transcriptomes in EBV-associated BLs and GCs to identify can-  
259 didate viral effectors in the natural tumor setting. Unlike lytic conditions, where 20% of expressed poly-ad-  
260 enylated RNAs in the cell are of viral origin (*Figure S2*), the sum of expressed latency transcripts in BLs  
261 and GCs does not exceed 0.02% of cellular RNAs (*Figure 1B, Figure S3*), with the majority of these being  
262 non-coding. Further, some of the EBV transcript signal in this analysis is derived from lytic gene expres-  
263 sion occurring in a minor population of tumor cells through occasional sporadic reactivation. Therefore,  
264 long RNA latency viral gene expression represents only a minor portion of the combined cell and viral tran-  
265 scriptome. We were unable to assess expression of the highly abundant non-polyadenylated small non-  
266 coding viral EBER1 and EBER 2 transcripts because the GC dataset was polyA-selected and because  
267 they are partially lost following RNA size selection in the ribodepletion-derived BL dataset (which results in  
268 unreliable quantifications across samples).

269 Housed within the most abundantly expressed viral polyadenylated RNA, the long non-coding RNA  
270 (lncRNA), RPMS1, are 20 densely clustered intronic pre-miRNAs encoding at least 31 mature miRNAs  
271 (*Figure 1C, Figure S4-5*). In contrast to the limited contribution of viral long RNAs to the tumor transcrip-  
272 tomes, the cumulative expression of viral miRNAs is remarkably high, exceeding host totals by as much as

273 3-fold (*Figure 1D*). This is particularly relevant because miRNA function is critically dependent on sufficient  
274 miRNA expression to saturate a high fraction of each target transcript. The importance of miRNA expres-  
275 sion levels on function is supported by previous studies that showed that poorly expressed miRNAs have  
276 little discernable biological activity(59) whereas sufficient expression of an individual miRNA can have a  
277 marked impact on tumor biology(60). The overwhelming expression of 31 viral miRNAs (*Figure 1D, Table*  
278 *S1*) in EBV-positive BLs and GCs supports their likely relevance in modulating the tumor transcriptome  
279 landscape.

280

281 **EBV miRNAs are over-represented in mRNA-bound RNA-induced silencing complexes (RISCs).**  
282 With the dependence on miRNA loading into RISC for target destabilization, the level of miRNA-RISC as-  
283 sociation is a predictor of miRNA targeting(61). To assess RISC association characteristics of EBV and  
284 host miRNAs, we performed a modified version(42) of Crosslinking, Ligation, And Sequencing of Hybrids  
285 (CLASH)(62), referred to as qCLASH(42), in EBV+ cell lines modeling BL (Akata) and GC (SNU719; *Fig-*  
286 *ure S6A*). In CLASH, each AGO-bound miRNA-mRNA pair is ligated and then sequenced as a contiguous  
287 read, reproducibly resolving both the diversity of miRNA targets as well as the relative abundance of each  
288 interaction (*Figure S6B*).

289 In conjunction with our qCLASH analyses, we also performed standard small RNA fraction se-  
290 quencing to assess the underlying expression of each miRNA in these cell lines. Notably, viral miRNA ex-  
291 pression in Akata and SNU719 cell lines was substantially lower than the levels observed in primary tu-  
292 mors (*Figure 2A-B, left*). Nevertheless, this finding is in-line with previous studies showing that EBV  
293 miRNA levels are low in cell lines (including SNU719 cells) but increase markedly upon passage in im-  
294 munocompromised mice(63, 64), likely due to an enhanced reliance on viral miRNAs in the *in vivo* setting.  
295 Despite the modest expression of viral miRNAs in *in vitro* cultured SNU719 and Akata cells, we found a  
296 remarkably high representation of EBV miRNA-mRNA hybrids (*Figure 2A-B, left*). This observed enrich-  
297 ment was not attributable to a limited number of individual viral miRNAs with unusually high binding effi-  
298 ciencies, but instead was a characteristic that was broadly attributable to the bulk of EBV miRNAs (*Figure*  
299 *2A-B, right*). These results indicate that in addition to exhibiting high *in vivo* expression, EBV miRNAs

300 evolved with feature(s) that enhance RISC formation, supporting the possibility of distinctly productive viral  
301 miRNA targeting.

302 To determine whether enhanced representation of viral miRNAs in RISC is a conserved feature of  
303  $\gamma$ HVs, we supplemented data from our previously published KSHV(42) and MHV68(65) qCLASH studies  
304 with small RNA sequencing to similarly compare KSHV and MHV68 hybrid levels to their respective  
305 miRNA expression. Similar to our findings with *in vitro* EBV miRNA expression, KSHV miRNAs were found  
306 to be expressed at low levels in KSHV infected LTC-TIVE cells (*Figure S7A*). Like our observations with  
307 EBV miRNAs, KSHV miRNAs exhibited marked enrichment in RISCs that was distributed across a spec-  
308 trum of KSHV miRNAs (*Figure S7A*). In contrast, an aggregate assessment of MHV68 miRNAs did not  
309 show over-representation within RISCs (*Figure S7B*). This lack of aggregate MHV68 miRNA enrichment in  
310 RISC, however, may be related to their non-canonical processing mechanisms(66). Nevertheless, at the  
311 individual miRNA level, we found that the two most overrepresented miRNAs within RISC in the MHV68-  
312 infected cell line, HE2.1, were the MHV68 M1-2-3p and M1-6-5p miRNAs (*Figure S7B, right*), suggesting  
313 that at least some MHV68 miRNAs are overrepresented in RISC. Together, these findings show prefer-  
314 tial loading of viral miRNAs into RISC across these three  $\gamma$ HVs, representing a possible common strategy  
315 to exert strong influences on infected cell transcriptomes.

316

### 317 **EBV miRNAs have high targeting efficacies.**

318 The disproportionately high association of viral miRNAs with RISCs could result from intrinsic properties of  
319 viral miRNAs that enhance loading into RISC. Nevertheless, high expression of viral miRNA and/or their  
320 targets could also contribute to the detection of greater numbers of miRNA-target RISCs. To account for  
321 the impact of miRNA and mRNA abundance on the level of AGO-bound miRNA-mRNA hybrids(67), we  
322 used an affinity constant calculation (dividing normalized hybrid counts by the normalized number of miR-  
323 NAs and mRNA target transcripts (*Figure 3C*)) as a quantitative metric for miRNA “targeting efficacy”. We  
324 first assessed how accurately this targeting efficacy metric reflects intrinsic properties of miRNAs rather  
325 than environmental, cell specific factors. Unlike cellular miRNAs, nearly all viral miRNA targets identified in  
326 Akata cells were also detected in SNU719 cells (*Figure 3A*), with the higher overall viral miRNA

327 expression in SNU719 accounting for the additional miRNA targets identified in this system. Despite the  
328 overlap of specific targets, the relative abundance of each viral miRNA-mRNA hybrid detected in both cell  
329 lines was poorly correlated (*Figure 3B*), likely due to the differences in mRNA and/or miRNA expression in  
330 SNU719 and Akata cells. In contrast, viral miRNA targeting efficacies were strongly correlated between  
331 cell lines (*Figure 3D*). This finding also extended to cell miRNAs using miRNA/target interactions found in  
332 both cell lines (*Figure 3D*). These data support our contention that this targeting efficacy metric is a quanti-  
333 tative measure of intrinsic properties of miRNAs and their target sites that influence RISC formation.

334 We next applied targeting efficacy measures to assess the innate RISC loading properties of viral  
335 and cellular miRNAs in Akata and SNU719 cells. Across each biological replicate, the targeting efficacy  
336 distributions were substantially higher for EBV miRNAs than cell miRNAs in both SNU719 and Akata cells  
337 (*Figure 3E, Table S2*). Extending this analysis to KSHV and MHV68 miRNAs, we similarly found that viral  
338 miRNAs have higher targeting efficacies than their cellular counterparts (*Figure S8A-B, Table S2*). These  
339 results indicate that the higher proportion of viral miRNAs in RISCs relative to their expression levels is  
340 due to intrinsic properties of viral miRNAs that influence target selection and RISC loading. This suggests  
341 that viral miRNAs have evolved to be more effective inhibitors of their mRNA targets than host miRNAs.

342

343 **EBV miRNAs target more accessible regions of mRNAs than cell miRNAs and form more thermo-  
344 dynamically stable hybrids.**

345 To assess biophysical properties underlying efficient viral miRNA RISC formation, we explored the nucleo-  
346 tide composition of miRNA/mRNA hybrids. Hybrid formation is guided in large part by the degree of com-  
347plementarity between bases 2-8 of miRNAs and their targets, with loading into RISC being further boosted  
348 by the presence of an “A” opposite the first base of the miRNA(68). These bases, collectively referred to  
349 as the “seed” region, display distinct complementarity patterns that are categorized into 9 different classes.  
350 With seed class being a known determinant of targeting effectiveness, we first tested whether there is a  
351 seed class bias for EBV miRNAs relative to cell miRNAs. As shown in *Figure S9*, there is no discernable  
352 enrichment of EBV miRNAs in seed classes with higher known targeting capabilities. Further, we found  
353 that within each seed class, viral miRNAs have higher targeting efficacies (*Figure 4A*). These data indicate  
354 that differential seed class utilization does not explain the increased targeting efficacy of EBV miRNAs.

355 In addition to the extent of seed matching, miRNA binding is improved when target sites are  
356 flanked by A/Us(69). Considering the 4 bases directly adjacent to the seed binding site (2 bases on each  
357 side of the seed binding region), we found that sites with high A/U content were associated with improved  
358 targeting efficacy for both cell and viral miRNAs (*Figure 4B, Figure S10A*). However, EBV, KSHV and  
359 MHV68 miRNAs tended to bind sites with fewer flanking A/Us (*Figure 4C, Figure S10B*), indicating that the  
360 number of flanking A/Us fails to explain the higher targeting efficacies of viral miRNAs.

361 Because secondary structure of target sites reduces accessibility and interferes with RISC for-  
362 mation(70), transcript regions with less intramolecular binding propensities are typically more effective  
363 miRNA targets. We therefore assessed target site accessibility for each CLASH hybrid using the RNAPl-  
364 fold(71) subpackage of the Vienna RNA suite using a window size and maximum base pairing separation  
365 of 80 and 40 bases, respectively. This analysis revealed that EBV miRNA target sites are, on average,  
366 more accessible than the target sites of host miRNAs (*Figure 4D*). This indicates that EBV miRNAs  
367 evolved to target more accessible regions of target RNAs providing one likely explanation for the observed  
368 higher targeting efficacies of EBV miRNAs.

369 The last feature that we assessed to determine the molecular basis of enhanced EBV miRNA-  
370 mRNA targeting efficacies was predicted minimum free energies of miRNA-mRNA hybrid pairs (across the  
371 entire miRNA and its target). This analysis revealed that EBV miRNA-mRNA hybrids tend to form more  
372 thermodynamically stable interactions than their cellular counterparts (*Figure 4E*). Extending this analysis  
373 to KSHV and MHV68 miRNAs, we found that like EBV miRNAs, targeting efficacies are higher for each  
374 seed class (not shown) and we found that KSHV and MHV68 miRNAs generally form more thermodynami-  
375 cally stable interactions than their cellular counterparts (*Figure S10C*). Together, these analyses indicate  
376 that  $\gamma$ HV miRNAs evolved with nucleotide sequence compositions that favor stronger hybrid interactions,  
377 providing another likely explanation for the enhanced targeting efficacy of viral miRNAs.

378

### 379 **EBV miRNAs have a greater impact on their targets than their cellular miRNA counterparts**

380 To test whether the higher overall targeting efficacies of EBV miRNAs translates to increased effective-  
381 ness in destabilizing their target mRNAs, we performed correlation analyses between the expression of  
382 each viral and cellular miRNA and their respective mRNA targets across EBV positive BL and GC

383 datasets. Correlations were displayed in cumulative distribution plots (*Figure 5*). Shifts in distributions from  
384 permuted correlations of the same set of miRNAs with random mRNA targets were analyzed using the  
385 Kolmogorov-Smirnov (KS) test (*Figure 5*). In both BLs and GCs, viral miRNAs showed strong inverse cor-  
386 relations with their targets (BL,  $p < 2.1 \times 10^{-6}$ ; GC,  $p < 1.2 \times 10^{-5}$ ). In contrast, correlations between human  
387 miRNAs and their targets were less pronounced and not statistically significant. These results provide *in*  
388 *vivo* evidence of functional impacts of EBV miRNAs on targets identified by CLASH and they show that the  
389 higher targeting efficacies of EBV miRNAs likely translates into stronger functional influences on their tar-  
390 gets.

391

## 392 **EBV miRNA target distributions**

393 In addition to assessing the impact that EBV miRNAs have on their individual targets, we also explored the  
394 breadth of viral miRNA targets to investigate the overall impact that EBV miRNAs have on the cell tran-  
395 scriptome. We first quantified the number of targets attributable to each viral miRNA (*Figure 6A*). Several  
396 viral miRNAs predominantly target a single transcript (for example, BART3-3p, BART17-3p, and BART20-  
397 5p), while others such as BART5-5p, BART7-3p, BART9-3p, and BART16 have many strong targets. The  
398 predicted seed-pairing stability (SPS; the predicted binding energy of positions 2-8 of a miRNA bound to  
399 its reverse complement target) of miRNAs is a predictor of how promiscuous the miRNA is(72) and these  
400 findings are borne out for EBV miRNAs. For example, BART7-3p (AUCAUAG;  $\Delta G^\circ = -5.53 \text{ kcal mol}^{-1}$ ),  
401 BART 9-3p (AACACUU;  $\Delta G^\circ = -5.54 \text{ kcal mol}^{-1}$ ), and BART16 (UAGAUAG;  $\Delta G^\circ = -5.73 \text{ kcal mol}^{-1}$ ; *Table*  
402 *S3*) have a relatively low SPS and extensively target a multitude of mRNAs ( $>100$  h.c.p.m.: BART7-3p,  
403 128; BART16, 35; BART9-3p, 25). BART5-5p (AAGGUGA;  $\Delta G^\circ = -7.98 \text{ kcal mol}^{-1}$ ) has an average SPS  
404 (ranking in the 48<sup>th</sup> percentile of all cellular miRNAs) and intermediate, 82 high abundance targets. MiR-  
405 NAs with high SPS, such as BART3-3p (GCACCAC;  $\Delta G^\circ = -11.29 \text{ kcal mol}^{-1}$ ), BART17-3p (GUAUGCC;  
406  $\Delta G^\circ = -9.37 \text{ kcal mol}^{-1}$ ), and BART20-5p (AGCAGGC;  $\Delta G^\circ = -11.53 \text{ kcal mol}^{-1}$ ), which have 11, 4, and 1  
407 high abundance target(s), respectively. These high SPS miRNAs tend to extensively target one transcript,  
408 with BART3-3p targeting IPO7 over 12-fold more often than its next most frequent interaction partner,  
409 BART17-3p:RBM8A accounting for nearly 8-fold more hybrids than its next best target, and BART20-

410 5p:UBE2H representing over 2-fold more hybrids than its next most common target. Overall, despite the  
411 relatively focused functions of some EBV miRNAs, EBV miRNAs as a whole tend to display greater  
412 breadth in targets than their cellular counterparts (*Figure 6B*). This may be a means through which EBV  
413 evolved to influence a larger target set despite having a smaller repertoire of encoded miRNAs.

414 While EBV miRNA targeting is generally spread across more transcripts, they tend to be directed  
415 towards transcripts regulated by fewer miRNAs (*Figure 6C*). This indicates that cellular miRNAs more of-  
416 ten work in a cooperative fashion. The higher targeting efficacies of viral miRNAs may reduce their re-  
417 quirement for cooperative targeting, as they tend to target a repertoire of transcripts that are distinct from  
418 cellular miRNAs. As an extension of their enhanced targeting efficacy, viral miRNAs are not constrained  
419 by the necessity of cooperative targeting, allowing them each to serve a unique purpose, and increasing  
420 their influence over host cell transcriptomes.

421

## 422 **EBV miRNAs interfere with immune signaling in the tumor microenvironment**

423 Next, we sought to investigate the potential functional impact of the most influential EBV miRNA-target in-  
424 teractions in modulating the host cell environment. Using the targets of the top 20 EBV miRNA-target inter-  
425 actions as network seed genes, we applied enrichR(53) to query pathway enrichment for each seed gene  
426 and its 20 strongest interacting partners. As a control, we performed a similar analysis on the targets of  
427 the top 20 cell miRNA-target interactions. This analysis revealed selective enrichment for Influenza and  
428 HIV infection, antigen processing and presentation (MHC class I), and IFN-stimulated genes and ISG15  
429 antiviral mechanisms as top EBV miRNA pathway hits (*Figure 6D, Table S4*). This suggests that the EBV  
430 miRNA-target interactions within the top 20 highest targeting efficacy interface with adaptive and innate  
431 immune response pathways.

432 Previous studies have shown that EBV positive GCs have higher immune cell infiltration than their  
433 EBV negative counterparts(73), likely due to sporadic expression of lytic viral proteins within the tumor.  
434 Using CIBERSORTx(74) to infer the immune cell infiltration in each tumor through deconvolution of im-  
435 mune cell signatures within the GC dataset (using only the microsatellite stable (MSS)-only cohort), we  
436 found higher levels of T-cell and macrophage subtypes in the EBV positive cohorts (*Figure S11A*). We  
437 also determined the diversity of infiltrating T-cells within these tumors by assessing the number of unique

438 T-cell receptor sequences for each tumor. Utilizing MIXCR(75), we realigned each tumor RNA-seq dataset  
439 to all potential combinations of rearranged T-cell receptors and used VDJTOOLS(76) for QC and T-cell  
440 clone quantifications. This analysis showed that consistent with the finding of higher levels of T-cell infiltration  
441 in EBV positive GCs through CIBERSORTx analysis, we found a greater diversity of T-cell clones in  
442 EBV positive tumors than in EBV negative tumors (*Figure S11B*). Together, these results confirm the find-  
443 ings of The Cancer Genome Atlas Research Network(56), showing that EBV likely induces some level of  
444 adaptive immune response in EBV positive GCs.

445 While the presence of EBV clearly induces immune cell infiltration into EBV associated tumors, we  
446 hypothesized that the interactions of viral miRNAs with immune regulatory pathways in infected cells acts  
447 as a counter measure to mitigate immune cell-mediated targeting of virus-infected tumor cells. To function-  
448 ally assess this possibility we first identified potential direct and indirect targets of viral miRNAs in the  
449 EBV+ BL and GC cohorts by correlating the sum of viral miRNA expression values with the expression  
450 levels of each cell gene (*Table S5*). Gene Set Enrichment Analysis (GSEA)(77, 78), using the pre-ranked  
451 BL and GC miRNA-gene correlations, revealed that viral miRNA expression negatively correlates with the  
452 IFN $\gamma$  and TNF $\alpha$  signaling pathways (*Figure 7A*). The inverse relationship between IFN $\gamma$  and TNF $\alpha$  signal-  
453 ing pathways and EBV miRNA expression suggests that EBV miRNAs mitigate IFN $\gamma$ - and TNF $\alpha$ - mediated  
454 amplification of the immune response. To more directly assess the relationship between EBV miRNAs and  
455 adaptive immune response, we used CIBERSORTx(74) to infer immune cell infiltration in each tumor sam-  
456 ple from the BL and GC datasets (*Table S6*). This analysis showed that CD8 T-cells, CD4 T-cells, and  
457 macrophages inversely correlate with viral miRNA expression (*Figure 7B*). Assessing the infiltrating T-cell  
458 diversity across these tumors showed a strong inverse correlation between unique T-cell clonotype counts  
459 and viral miRNA expression (*Figure 7C, Table S7*), further supporting a role of EBV miRNAs in interfering  
460 with the immune response to EBV infection within these tumors. These findings are most tightly associ-  
461 ated with EBV miRNAs rather than other expressed EBV transcripts since EBV miRNAs show a stronger  
462 inverse relationship with T-cell clonotype numbers than viral pol II transcripts (*Figure S12*). Together these  
463 analyses provide evidence that the targeting of components of immune response pathways by EBV

464 miRNAs results in the dampening of innate and adaptive immune responses to viral infection in EBV posi-  
465 tive cancers.  
466

467 **DISCUSSION**

468

469 By integrating miRNA and mRNA expression levels with hybrid quantifications obtained via CLASH, we  
470 used an affinity constant calculation to assess targeting efficacy for each interaction. Comparing targeting  
471 efficacies of viral and host miRNA-target interactions, we found that viral miRNAs generally bind their tar-  
472 gets more effectively than host miRNAs. The elevated efficacy of EBV miRNA-mRNA interactions trans-  
473 cended seed match and the level of flanking AU content. Instead, we found that the complexes formed be-  
474 tween EBV miRNAs and their targets were more thermodynamically stable and tended to occur at target  
475 sites with less secondary structure. In metazoans, broadly conserved miRNA target sites tend to facilitate  
476 the most effective targeting interactions. However, these sites exhibit a negative selection over time that  
477 tempers miRNA binding efficacy. Unlike targets of broadly expressed miRNAs, co-expressed targets of  
478 miRNAs that exhibit tissue specific expression tend to evolve effectiveness-reducing alterations in target  
479 sites(79), suggesting that the major role of miRNAs is to fine-tune gene expression rather than to signifi-  
480 cantly alter it(80). The continued coevolution of cell miRNAs and their target genes presents an internal  
481 arms race that ultimately reduces the impact of the majority of miRNA-mRNA interactions. These con-  
482 straints do not apply to viral miRNAs which have evolved to effectively target a large number of host tran-  
483 scripts, with some miRNAs such as BART7-3p effectively binding many target mRNAs, and others, such  
484 as BART3-3p, homing in on a single transcript (notably, this latter class of viral miRNA might implicate sin-  
485 gular targets that are critical to viral persistence and/or expansion in host cells, potentially presenting a  
486 vulnerability to the virus). The tendency of viral miRNAs to exhibit high targeting efficacies therefore arm  
487 them with the unmatched ability to influence the landscape of host RNA expression.

488 A longstanding challenge in deciphering miRNA function is the accurate assessment of its tar-  
489 gets(81). Because the most favorable interactions require only 7 bases of complementarity, even the most  
490 infrequent 3' UTR binding motifs are widely dispersed throughout the transcriptome. Still, the number of  
491 true miRNA binding sites is at least an order of magnitude lower than the number of seed complementary  
492 sequences in transcriptome 3' UTRs. The ability to discern true miRNA targets has improved dramatically  
493 with the advent and continued development of binding site prediction algorithms(69, 81), and even more  
494 so with high throughput experimental approaches such as PAR-CLIP(82). These tools have seeded

495 studies of EBV miRNA functions, leading to the discovery of consequential mRNA targets(83) including  
496 mediators of apoptotic signaling, BBC3 (BART5-5p)(84) and BAD (BART20-5p)(85) and regulators of in-  
497 nate immunity, NDRG1 (multiple)(86), IL12A (BART?), MICB (BART2-5p)(87), IFI30 (BART1 and BART2),  
498 LGMN (BART1 and BART2), and CTSB (BART1 and BART2)(88). However, both putative and empirically  
499 identified viral miRNA targets have often been difficult to validate(89). In our system, the BBC3 interaction  
500 was the 220<sup>th</sup> most prevalent hybrid of BART5-5p (38 h.c.p.m.), CTSB was the 375<sup>th</sup> most abundant  
501 BART1-5p target (6 h.c.p.m.), and combined, NDRG1 hybrids ranked 3681<sup>st</sup> among all viral miRNA targets  
502 (25 h.c.p.m.). We were unable to detect any viral miRNA hybrids with IFI30, LGMN, or BAD, while MICB  
503 and IL12A were not sufficiently expressed in SNU719 cells. Overall, little overlap exists between targets  
504 identified among previously published high throughput EBV miRNA targetome studies(89), yet, one con-  
505 sistently identified interaction is that between BART3-3p and IPO7, an interaction that has subsequently  
506 been used as a control in studies of EBV miRNA targeting(35, 90), we detect substantial levels of this in-  
507 teraction (6846 h.c.p.m.; ranked 1<sup>st</sup> among BART3-3p targets), suggesting the quantitative nature of this  
508 approach helps distinguish the targets of both viral and host miRNAs that are likely to be impacted the  
509 most.

510 Among the most frequent targets of several EBV miRNAs were transcripts coding for ubiquitin lig-  
511 ases and adapters. These include the E3 ubiquitin ligases, FBXO21 (BART21-5p; ranked 1<sup>st</sup> among all  
512 BART21-5p interactions), TRIM65 (BART7-3p; ranked 5<sup>th</sup>), RNF38 (BART5-5p; ranked 7<sup>th</sup>), TRIM8  
513 (BART16; ranked 1<sup>st</sup>), and KCMF1 (BART1-3p; ranked 2<sup>nd</sup> and BART3-3p; ranked 2<sup>nd</sup>), the E2 ubiquitin  
514 ligase, UBE2H (BART20-5p; ranked 1<sup>st</sup> and BART7-3p; ranked 17<sup>th</sup>), and the E3 ubiquitin ligase adapters,  
515 BTBD1 (BART5-5p; ranked 1<sup>st</sup>) and UBXN7 (BART5-5p; ranked 16<sup>th</sup>). Several of these ubiquitin ligases  
516 have important roles in host intrinsic immunity against viral infection. Both FBXO21 and TRIM65 are nec-  
517 essary for the production of type I IFNs in response to viral infection(91, 92). TRIM8 is a potent activator of  
518 TNF $\alpha$  and NFKB signaling(93), both pathways of which we found to have a strong inverse correlation with  
519 viral miRNAs in BLs and GCs (*Figure 7A*).

520 A more general possible functional consequence of inhibiting ubiquitin ligase expression is interfer-  
521 ence with MHC class I antigen presentation. Previous studies have shown that EBV miRNAs collectively  
522 reduce host cell antigen presentation, culminating in the subversion of CD4+ and CD8+ T-cell

523 surveillance(88, 94, 95). Numerous viruses have evolved various mechanisms to interfere with this path-  
524 way. For example, the HIV NEF protein redirects HLA-A and HLA-B transportation(96), the Hepatitis B Vi-  
525 rus X protein interferes with proteasomal activity(97), K3 and K5 of KSHV promote MHC-I endocytosis and  
526 destruction(98), MHV68 MK3 is a ubiquitin ligase that targets MHC-I for destruction(99), and both the U6  
527 protein of HCMV and EBV encoded BNLF2A inhibit TAP-mediated peptide transport and subsequent MHC  
528 loading(100-102). While viral protein expression is restricted in EBV-associated tumors, the presence of  
529 the virus still elicits an immune response and mutations that help drive tumors produce neo-epitopes that  
530 immune cells may recognize as foreign. The survival of EBV positive cells, including tumors, therefore, re-  
531 quires immune subversion or escape(103). Previous studies have shown that EBV miRNA expression is  
532 elevated by inoculation of tissue culture grown EBV positive tumor cells in mice(104). Furthermore, we  
533 found that EBV miRNAs inversely correlate with immune cell infiltrates in BLs and GCs, suggesting that an  
534 important role of the viral miRNAs is to interfere with immune surveillance, thereby helping facilitate the  
535 survival and expansion of the underlying tumor.

536       Altogether, our findings show that EBV miRNAs are uniquely effective inhibitors of target RNAs  
537 through facilitating high *in vivo* expression and the targeting of accessible sites with more favorable  
538 miRNA/target binding energies, thereby achieving conserved impacts on immune responses to infected  
539 tumor cell populations.

540

## 541 **AVAILABILITY**

542 All source code is available in our GitHub repository ([https://github.com/flemingtonlab/ebv\\_clash](https://github.com/flemingtonlab/ebv_clash)).

543

## 544 **ACCESSION NUMBERS**

545 Small fraction and CLASH sequences have been deposited to the NCBI Gene Expression Omnibus  
546 ([GSE147228](https://www.ncbi.nlm.nih.gov/geo/query/acc.cgi?acc=GSE147228)). Accession numbers for polyA-selected RNA sequencing reads are [GSM1267812](https://www.ncbi.nlm.nih.gov/geo/query/acc.cgi?acc=GSM1267812)  
547 (Akata)(105) and [GSM1104509](https://www.ncbi.nlm.nih.gov/geo/query/acc.cgi?acc=GSM1104509) (SNU719)(73).

548

549

550

551 **FUNDING**

552 This work was supported by the National Institutes of Health [R01CA243793, R21CA236549 to E.K.F.,  
553 P01CA214091 to E.K.F., S.T., R.R.], and the Lymphoma Research Foundation (N.U.).

554

555 **AUTHOR CONTRIBUTIONS**

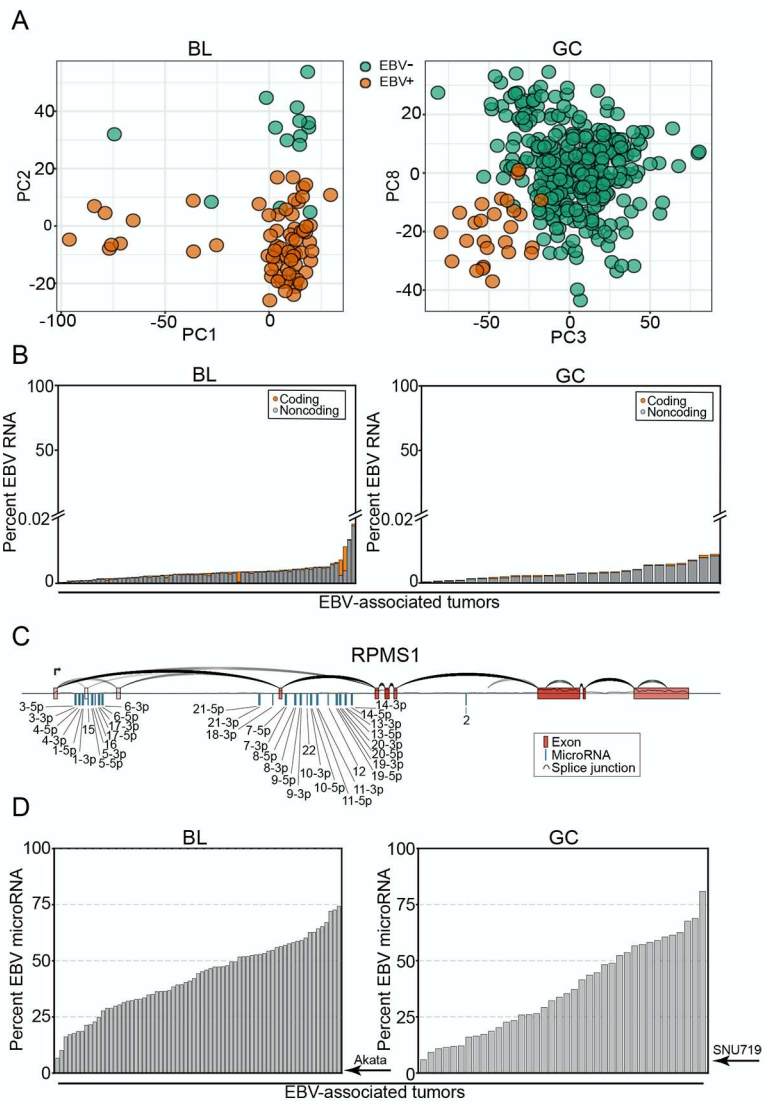
556 E.K.F., S.T., R.R., and N.A.U. conceived the project; W.B., and M.K. performed the CLASH experiments,  
557 N.A.U., and E.K.F. wrote the scripts, processed and analyzed the data, and wrote and edited the manu-  
558 script.

559

560 **CONFLICT OF INTEREST**

561 The authors declare they have no competing interests.

562



563

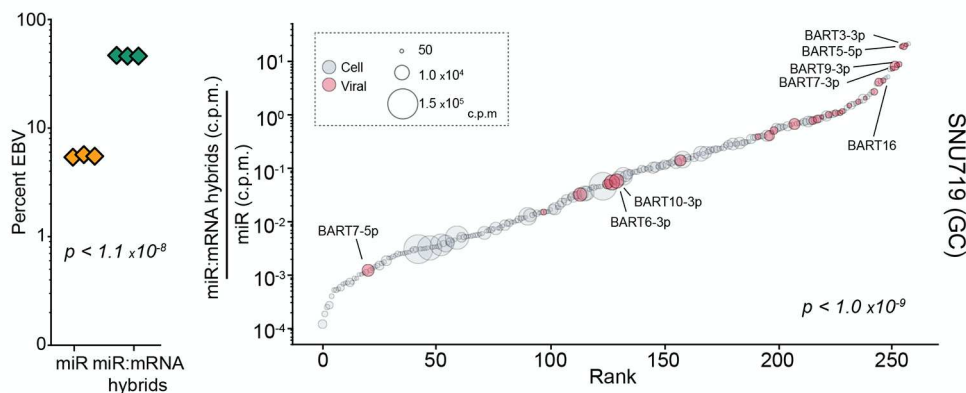
564

565 **Figure 1. High expression of viral miRNAs in EBV-associated tumors.** Raw RNA sequencing reads  
566 were obtained from the Burkitt Lymphoma Genome Sequencing Project(106) (BL; N=84) and The Cancer  
567 Genome Atlas(58) (GC; N=235). Samples were aligned to the combined human (GENCODE  
568 GRCh38.p13)(44) and EBV(45) transcriptomes. (A) Principle component analysis (PCA) of BL and GC  
569 gene expression. (B) The viral percentage of total gene expression in each tumor sample,  
570  $\frac{\Sigma \text{viral transcripts (t.p.m.)}}{10^6}$ . (C) The structure of the EBV RPMS1 locus, including the BART miRNA clusters,  
571 plotted with SpliceV(107). The coverage track and splice junction counts were derived from the aligned  
572 RNA-Seq reads of an EBV<sup>+</sup> BL patient (BLGSP-71-06-00281). (D) The viral percentage of total miRNA

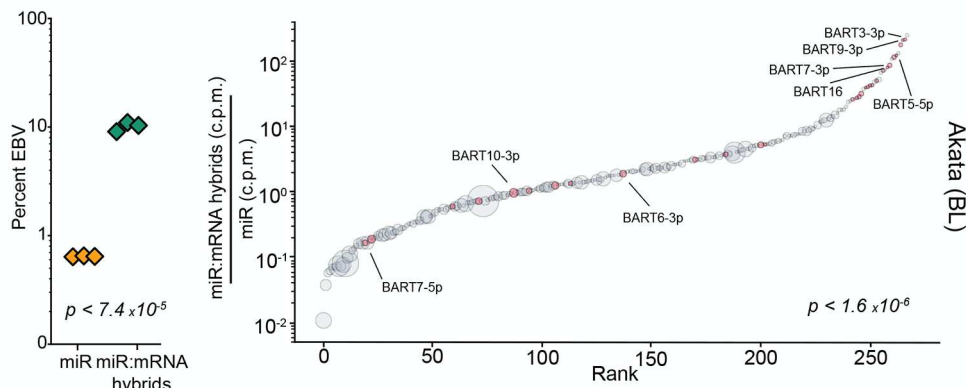
573 expression in each tumor sample,  $\frac{\sum \text{viral microRNA (c.p.m.)}}{10^6}$ . Akata and SNU719 labels indicate the viral per-

574 centage of reads in Akata and SNU719 cell lines.

A



B

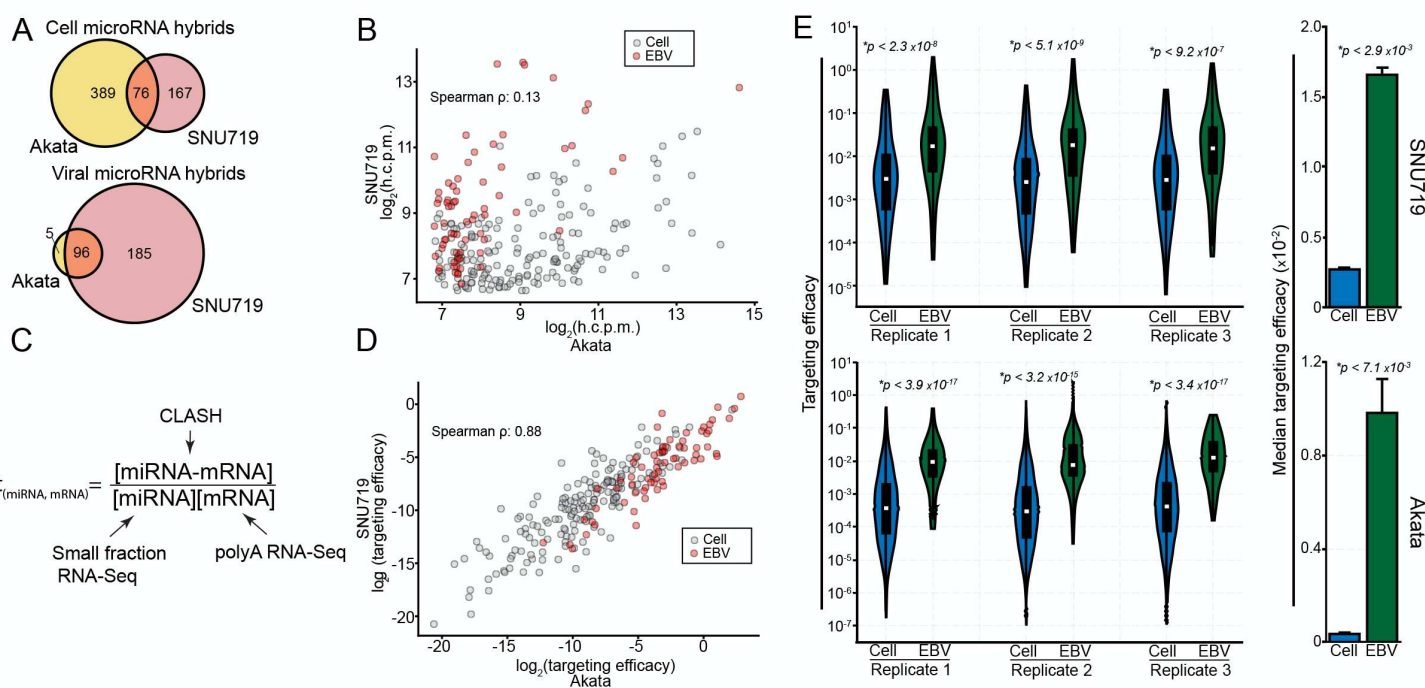


575

576

577

578 **Figure 2. EBV miRNAs are over-represented in RNA induced silencing complexes (RISCs).** CLASH  
 579 and miRNA-sequencing were performed in triplicate for SNU719 and Akata cells. (A-B, left) The viral per-  
 580 centage of total miRNA expression in each sample,  $\frac{\sum \text{viral microRNA (c.p.m.)}}{10^6}$  (yellow triangles), and the per-  
 581 centage of all miRNA-mRNA hybrids containing a viral miRNA,  $\frac{\sum \text{viral microRNA:mRNA hybrids (h.c.p.m.)}}{10^6}$  (green trian-  
 582 gles), were calculated. The indicated P-values were calculated using unpaired Student's t-tests. (A-B,  
 583 right) The average number of miRNA-mRNA hybrids formed for each miRNA was normalized to its base-  
 584 line expression level,  $\frac{\text{microRNA}_x:\text{mRNA hybrids (h.c.p.m.)}}{\text{microRNA}_x \text{ (c.p.m.)}}$ . These mRNA-bound proportions were plotted in order  
 585 of rank on the corresponding x-axis. Each circle represents an individual miRNA; circle size represents  
 586 expression level; red circles indicate viral miRNAs. The indicated P-values were calculated using the Kol-  
 587 mogorov-Smirnov test (KS), comparing viral and human miRNAs.

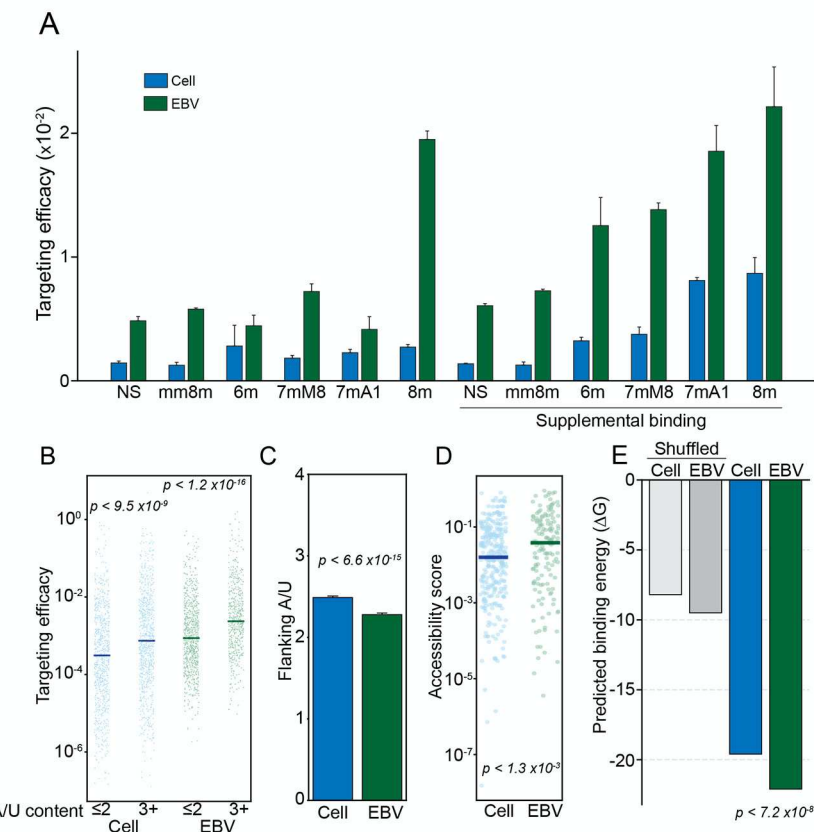


588

589

590

591 **Figure 3. EBV miRNAs have high targeting efficacy.** (A) Venn diagrams comparing genes found to be  
 592 targeted in Akata and SNU719 cells by cellular (top) and viral (bottom) miRNAs. Only high confidence tar-  
 593 gets (on average  $>100$  h.c.p.m.) were considered. (B) h.c.p.m values for each interaction pair were com-  
 594 pared between Akata and SNU719 cells, considering all interactions found in both cell lines. The  $\log_2$ -  
 595 transformed values from each cell line were correlated, resulting in a correlation coefficient of  $p = 0.13$   
 596 (Spearman). (C) Schematic of the targeting efficacy calculation. (D) The  $\log_2$ -transformed targeting effic-  
 597 acies were correlated between SNU719 and Akata cells, resulting in a spearman correlation coefficient of  $p$   
 598 = 0.81. (E; left) The distribution of targeting efficacies for each interaction in each CLASH replicate, com-  
 599 paring viral and cellular interactions. P-values were calculated using the KS test. (E; right) The median tar-  
 600 geting efficacy of all three replicates. P-values were calculated using paired Student's t-tests.

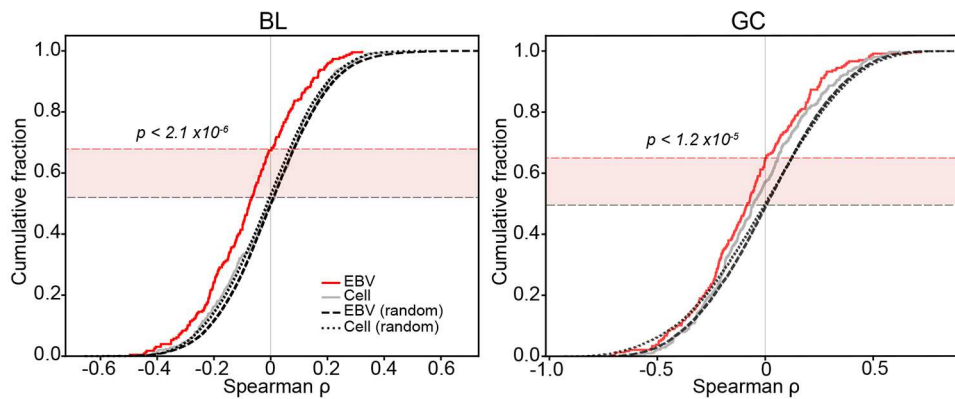


601

602

603 **Figure 4. EBV miRNA hybrids are thermodynamically stable.** Interactions were categorized by seed  
604 match type (NS, no seed; mm8m, mismatch 8mer; 6m, 6mer; 7mM8, 7mer base 8 match; 7mA1, 7mer A1  
605 (A opposite base 1); 8m, 8mer), with “supplemental” interactions requiring >3 bases of complementarity  
606 between bases 13-17 of the miRNA and its target. (A) Median targeting efficacy for each type of seed  
607 match comparing viral and cellular miRNA interactions. (B) The targeting efficacy of each interaction  
608 binned by flanking A/U content of each miRNA target site. The two most proximal bases on each side of  
609 the seed binding region were considered. P-values were calculated using the KS test. (C) The mean num-  
610 ber of flanking A/Us (max = 4) for cell and EBV miRNA target sites. P value was calculated via KS test. (D)  
611 The predicted local site accessibility score of each miRNA target site, using RNAPlfold (-W 80 -L 40 -u).  
612 The scores indicate the probability that all 14 bases, centered on position 7 of the miRNA target site, will  
613 be unpaired. P-values were calculated using the KS test. (E) Predicted minimum free binding energies  
614 (ΔG) were calculated for each hybrid using the RNAcofold function of the Vienna RNA Suite(108). As a

615 control,  $\Delta G$  calculations were performed on shuffled sequences, with 100 permutations performed for each  
616 hybrid pair. The  $\Delta G$  values of cellular and viral hybrids were compared by KS test.  
617

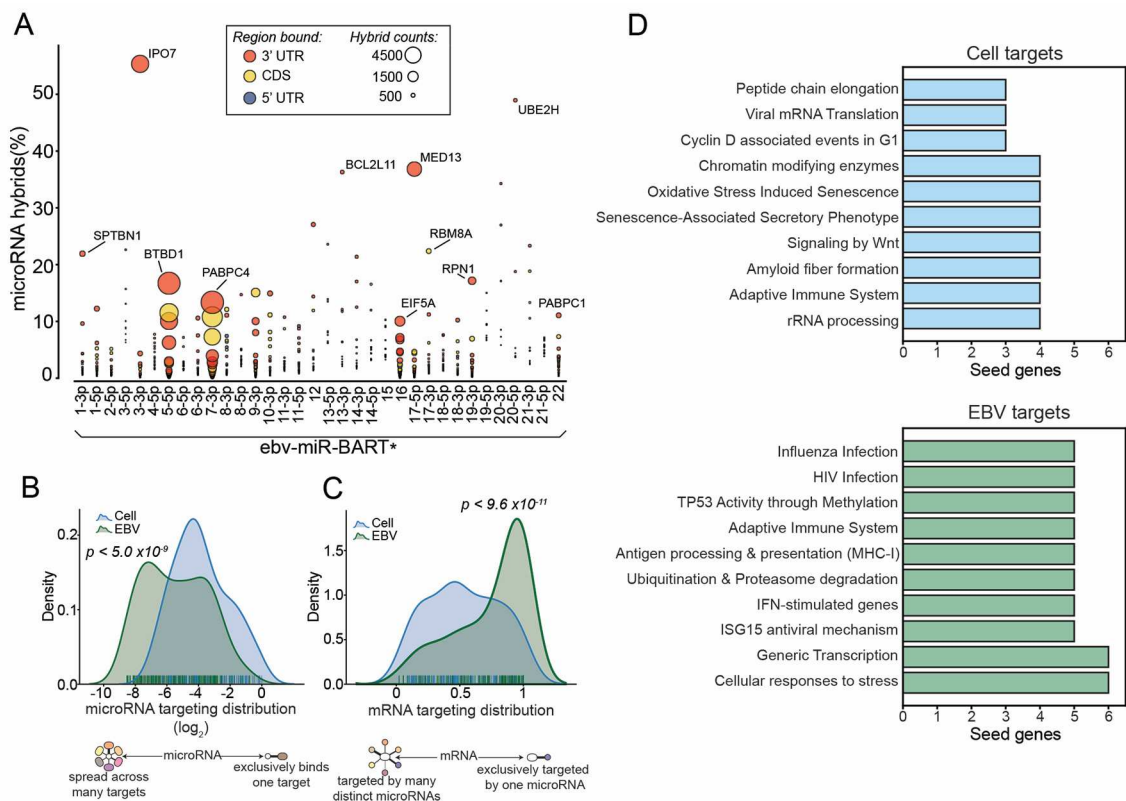


618

619

620 **Figure 5. EBV miRNAs and their targets have strong inverse correlations in primary BLs and GCs.**

621 For each CLASH miRNA-mRNA hybrid, mRNA and miRNA expression levels (c.p.m.) were correlated  
622 across all EBV-positive BL and GC tumors. Correlations were performed on hybrids that met the following  
623 criteria: 1. Average miRNA expression in tumors  $\geq 10$  c.p.m., 2. Average mRNA expression in tumors  $> 5$   
624 t.p.m., 3.  $\frac{h.c.p.m.}{mRNA\ t.p.m.} > 3$ , and 4. miRNA-mRNA interactions occurred within the 3'-UTR, where miRNA me-  
625 diated repression is more often effective(109). Cumulative distribution plots were generated using ranked  
626 Spearman correlation coefficients for each species. As a control, expression levels of the miRNA of each  
627 hybrid pair analyzed was correlated with expression levels of a random mRNA across the same tumors.  
628 For each randomized interaction, 100 permutations were run. Correlation values of EBV miRNA-mRNA  
629 pairs were compared to randomized controls; P-values were generated using the KS test.

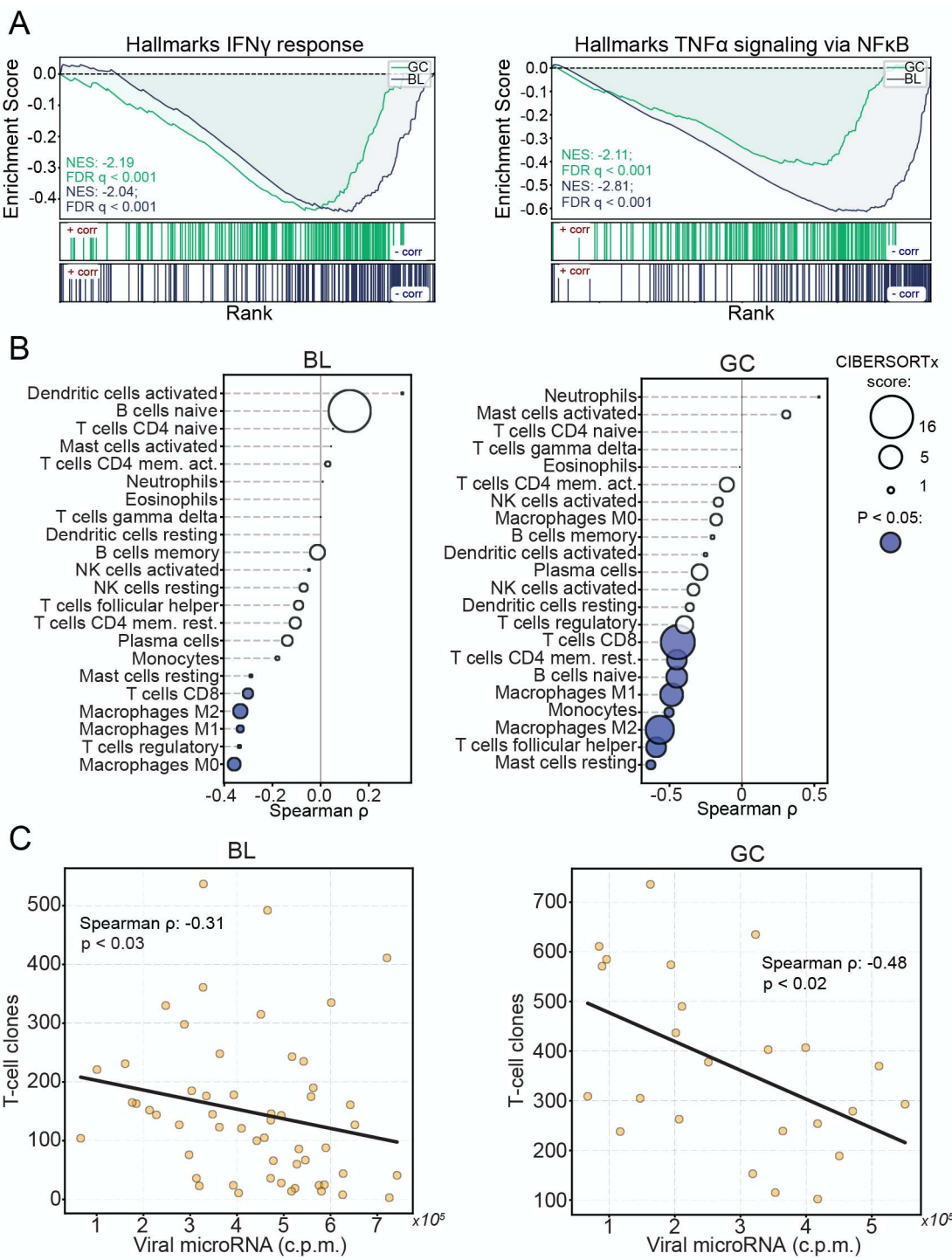


630

631

632 **Figure 6.  $\gamma$ HV miRNAs target components of the ubiquitin-proteasome system.**

633 (A) SNU719 hybrids containing EBV miRNAs. Each interaction was represented by a circle; circle size  
 634 corresponds to the total number of hybrids formed ( $microRNA_x:mRNA_y$  h.c.p.m); The y-axis values  
 635 represent the percent of all hybrids that contain the indicated miRNA,  $\frac{microRNA_x-mRNA_y \text{ h.c.p.m.}}{\sum microRNA_n-mRNA_y \text{ h.c.p.m.}}$ . (B) The  
 636 distribution of y-axis values from (A), extended to all hybrids. Cellular and viral hybrids were compared; P-  
 637 value was generated using the KS test. (C) The fraction of individual miRNAs hybridizing with each mRNA,  
 638  $\frac{microRNA_x-mRNA_y \text{ h.c.p.m.}}{\sum microRNA_n-mRNA_y \text{ h.c.p.m.}}$ , comparing viral and human distributions; P-value was generated using the KS  
 639 test. (D) Pathways targeted by EBV and cellular target genes. Protein-protein interaction networks of each  
 640 of the top 20 EBV or cellular target genes were obtained from StringDB(52), and resulting protein names  
 641 were submitted to Enrichr(53) for pathway enrichment analysis (interrogating pathways included in the  
 642 Reactome database). All statistically significant pathways (FDR < 0.05) were assigned to the target gene.



643

644

645 **Figure 7. Viral miRNAs interfere with anti-viral immunity.** The sum of all viral miRNA c.p.m. was  
 646 correlated to expression levels of each mRNA (c.p.m.) in EBV-positive BL and GC tumors. The  
 647 correlations were ranked, then gene lists were interrogated using GSEA. (A) Stacked GSEA curves of the  
 648 Hallmarks IFNy signaling pathway (left) and the TNF $\alpha$ -NF $\kappa$ B signaling pathway (right). NES, nominal  
 649 enrichment score, FDR, false discovery rate. (B) Immune cell infiltrates were inferred using CIBERSORTx.

650 Each cell type was correlated (spearman) to the sum of EBV miRNAs across EBV-positive BLs and GCs.

651 Circle size represents the average CIBERSORTx absolute score across all tumors, filled circles represent

652 statistically significant ( $P < 0.05$ ) spearman correlations. (C) T-cell clonotypes were obtained for each EBV-

653 positive tumor sample using MIXCR; The number of unique clonotypes was correlated with the sum of

654 viral miRNAs in EBV-positive BLs and GCs.

655

656 **REFERENCES**

657

658 1. Epstein MA, Achong BG, Barr YM. Virus Particles in Cultured Lymphoblasts from Burkitt's  
659 Lymphoma. *Lancet*. 1964;1(7335):702-3.

660 2. Xiong J, Cui BW, Wang N, Dai YT, Zhang H, Wang CF, et al. Genomic and Transcriptomic  
661 Characterization of Natural Killer T Cell Lymphoma. *Cancer Cell*. 2020;37(3):403-19 e6.

662 3. Oyama T, Yamamoto K, Asano N, Oshiro A, Suzuki R, Kagami Y, et al. Age-related EBV-  
663 associated B-cell lymphoproliferative disorders constitute a distinct clinicopathologic group: a  
664 study of 96 patients. *Clin Cancer Res*. 2007;13(17):5124-32.

665 4. Hjalgrim H, Askling J, Rostgaard K, Hamilton-Dutoit S, Frisch M, Zhang JS, et al.  
666 Characteristics of Hodgkin's lymphoma after infectious mononucleosis. *N Engl J Med*.  
667 2003;349(14):1324-32.

668 5. zur Hausen H, Schulte-Holthausen H, Klein G, Henle W, Henle G, Clifford P, et al. EBV  
669 DNA in biopsies of Burkitt tumours and anaplastic carcinomas of the nasopharynx. *Nature*.  
670 1970;228(5276):1056-8.

671 6. Shibata D, Weiss LM. Epstein-Barr virus-associated gastric adenocarcinoma. *Am J Pathol*.  
672 1992;140(4):769-74.

673 7. Messick TE, Smith GR, Soldan SS, McDonnell ME, Deakyne JS, Malecka KA, et al.  
674 Structure-based design of small-molecule inhibitors of EBNA1 DNA binding blocks Epstein-Barr  
675 virus latent infection and tumor growth. *Science Translational Medicine*. 2019;11(482).

676 8. Munz C. Latency and lytic replication in Epstein-Barr virus-associated oncogenesis. *Nat  
677 Rev Microbiol*. 2019;17(11):691-700.

678 9. Chijioke O, Muller A, Feederle R, Barros MH, Krieg C, Emmel V, et al. Human natural killer  
679 cells prevent infectious mononucleosis features by targeting lytic Epstein-Barr virus infection. *Cell  
680 Rep*. 2013;5(6):1489-98.

681 10. Henderson S, Rowe M, Gregory C, Croom-Carter D, Wang F, Longnecker R, et al.

682 Induction of bcl-2 expression by Epstein-Barr virus latent membrane protein 1 protects infected B

683 cells from programmed cell death. *Cell*. 1991;65(7):1107-15.

684 11. Kilger E, Kieser A, Baumann M, Hammerschmidt W. Epstein-Barr virus-mediated B-cell

685 proliferation is dependent upon latent membrane protein 1, which simulates an activated CD40

686 receptor. *EMBO J*. 1998;17(6):1700-9.

687 12. Yin Y, Manoury B, Fahraeus R. Self-inhibition of synthesis and antigen presentation by

688 Epstein-Barr virus-encoded EBNA1. *Science*. 2003;301(5638):1371-4.

689 13. Kuppers R. B cells under influence: transformation of B cells by Epstein-Barr virus. *Nat*

690 *Rev Immunol*. 2003;3(10):801-12.

691 14. Raab-Traub N. Epstein-Barr virus in the pathogenesis of NPC. *Semin Cancer Biol*.

692 2002;12(6):431-41.

693 15. Kennedy G, Komano J, Sugden B. Epstein-Barr virus provides a survival factor to Burkitt's

694 lymphomas. *Proceedings of the National Academy of Sciences*. 2003;100(24):14269-74.

695 16. Tempera I, De Leo A, Kossenkov AV, Cesaroni M, Song H, Dawany N, et al. Identification

696 of MEF2B, EBF1, and IL6R as Direct Gene Targets of Epstein-Barr Virus (EBV) Nuclear Antigen

697 1 Critical for EBV-Infected B-Lymphocyte Survival. *Journal of Virology*. 2016;90(1):345-55.

698 17. Ballestas ME, Chatis PA, Kaye KM. Efficient persistence of extrachromosomal KSHV DNA

699 mediated by latency-associated nuclear antigen. *Science*. 1999;284(5414):641-4.

700 18. Hammerschmidt W, Sugden B. Identification and characterization of oriLyt, a lytic origin of

701 DNA replication of Epstein-Barr virus. *Cell*. 1988;55(3):427-33.

702 19. van Santen V, Cheung A, Kieff E. Epstein-Barr virus RNA VII: size and direction of

703 transcription of virus-specified cytoplasmic RNAs in a transformed cell line. *Proc Natl Acad Sci U*

704 *S A*. 1981;78(3):1930-4.

705 20. Brooks LA, Lear AL, Young LS, Rickinson AB. Transcripts from the Epstein-Barr virus  
706 BamHI A fragment are detectable in all three forms of virus latency. *J Virol.* 1993;67(6):3182-90.

707 21. Ungerleider N, Concha M, Lin Z, Roberts C, Wang X, Cao S, et al. The Epstein Barr virus  
708 circRNAome. *PLoS Pathog.* 2018;14(8):e1007206.

709 22. Toptan T, Abere B, Nalesnik MA, Swerdlow SH, Ranganathan S, Lee N, et al. Circular  
710 DNA tumor viruses make circular RNAs. *Proc Natl Acad Sci U S A.* 2018;115(37):E8737-E45.

711 23. Bullard WL, Flemington EK, Renne R, Tibbetts SA. Connivance, Complicity, or Collusion?  
712 The Role of Noncoding RNAs in Promoting Gammaherpesvirus Tumorigenesis. *Trends Cancer.*  
713 2018;4(11):729-40.

714 24. Bartel DP. Metazoan MicroRNAs. *Cell.* 2018;173(1):20-51.

715 25. Liu W, Wang X. Prediction of functional microRNA targets by integrative modeling of  
716 microRNA binding and target expression data. *Genome Biology.* 2019;20(1).

717 26. Hu W, Dooley J, Chung SS, Chandramohan D, Cimmino L, Mukherjee S, et al. miR-29a  
718 maintains mouse hematopoietic stem cell self-renewal by regulating Dnmt3a. *Blood.*  
719 2015;125(14):2206-16.

720 27. Choi YJ, Lin CP, Ho JJ, He X, Okada N, Bu P, et al. miR-34 miRNAs provide a barrier for  
721 somatic cell reprogramming. *Nat Cell Biol.* 2011;13(11):1353-60.

722 28. Welch C, Chen Y, Stallings RL. MicroRNA-34a functions as a potential tumor suppressor  
723 by inducing apoptosis in neuroblastoma cells. *Oncogene.* 2007;26(34):5017-22.

724 29. Lu LF, Boldin MP, Chaudhry A, Lin LL, Taganov KD, Hanada T, et al. Function of miR-  
725 146a in controlling Treg cell-mediated regulation of Th1 responses. *Cell.* 2010;142(6):914-29.

726 30. Rodriguez A, Vigorito E, Clare S, Warren MV, Couttet P, Soond DR, et al. Requirement of  
727 bic/microRNA-155 for normal immune function. *Science.* 2007;316(5824):608-11.

728 31. Zhu JY, Pfuhl T, Motsch N, Barth S, Nicholls J, Grasser F, et al. Identification of novel  
729 Epstein-Barr virus microRNA genes from nasopharyngeal carcinomas. *J Virol.* 2009;83(7):3333-  
730 41.

731 32. Grundhoff A, Sullivan CS, Ganem D. A combined computational and microarray-based  
732 approach identifies novel microRNAs encoded by human gamma-herpesviruses. *RNA.*  
733 2006;12(5):733-50.

734 33. Zhu JY, Strehle M, Frohn A, Kremmer E, Hofig KP, Meister G, et al. Identification and  
735 Analysis of Expression of Novel MicroRNAs of Murine Gammaherpesvirus 68.  
736 2010;84(19):10266-75.

737 34. Kozomara A, Birgaoanu M, Griffiths-Jones S. miRBase: from microRNA sequences to  
738 function. *Nucleic Acids Research.* 2019;47(D1):D155-D62.

739 35. Skalsky RL, Corcoran DL, Gottwein E, Frank CL, Kang D, Hafner M, et al. The viral and  
740 cellular microRNA targetome in lymphoblastoid cell lines. *PLoS Pathog.* 2012;8(1):e1002484.

741 36. Haecker I, Gay LA, Yang Y, Hu J, Morse AM, McIntyre LM, et al. Ago HITS-CLIP expands  
742 understanding of Kaposi's sarcoma-associated herpesvirus miRNA function in primary effusion  
743 lymphomas. *PLoS Pathog.* 2012;8(8):e1002884.

744 37. Gottwein E, Corcoran DL, Mukherjee N, Skalsky RL, Hafner M, Nusbaum JD, et al. Viral  
745 microRNA targetome of KSHV-infected primary effusion lymphoma cell lines. *Cell Host Microbe.*  
746 2011;10(5):515-26.

747 38. Kang D, Skalsky RL, Cullen BR. EBV BART MicroRNAs Target Multiple Pro-apoptotic  
748 Cellular Genes to Promote Epithelial Cell Survival. *PLoS Pathog.* 2015;11(6):e1004979.

749 39. Barth S, Pfuhl T, Mamiani A, Ehses C, Roemer K, Kremmer E, et al. Epstein-Barr virus-  
750 encoded microRNA miR-BART2 down-regulates the viral DNA polymerase BALF5. *Nucleic Acids  
751 Res.* 2008;36(2):666-75.

752 40. Hooykaas MJG, van Gent M, Soppe JA, Kruse E, Boer IGJ, van Leenen D, et al. EBV  
753 MicroRNA BART16 Suppresses Type I IFN Signaling. *J Immunol.* 2017;198(10):4062-73.

754 41. Helwak A, Kudla G, Dudnakova T, Tollervey D. Mapping the human miRNA interactome by  
755 CLASH reveals frequent noncanonical binding. *Cell.* 2013;153(3):654-65.

756 42. Gay LA, Sethuraman S, Thomas M, Turner PC, Renne R. Modified Cross-Linking,  
757 Ligation, and Sequencing of Hybrids (qCLASH) Identifies Kaposi's Sarcoma-Associated  
758 Herpesvirus MicroRNA Targets in Endothelial Cells. *J Virol.* 2018;92(8).

759 43. Grossman RL, Heath AP, Ferretti V, Varmus HE, Lowy DR, Kibbe WA, et al. Toward a  
760 Shared Vision for Cancer Genomic Data. *New England Journal of Medicine.* 2016;375(12):1109-  
761 12.

762 44. Frankish A, Diekhans M, Ferreira A-M, Johnson R, Jungreis I, Loveland J, et al.  
763 GENCODE reference annotation for the human and mouse genomes. *Nucleic Acids Research.*  
764 2019;47(D1):D766-D73.

765 45. O'Grady T, Wang X, Honer Zu Bentrup K, Baddoo M, Concha M, Flemington EK. Global  
766 transcript structure resolution of high gene density genomes through multi-platform data  
767 integration. *Nucleic Acids Res.* 2016;44(18):e145.

768 46. Bray NL, Pimentel H, Melsted P, Pachter L. Near-optimal probabilistic RNA-seq  
769 quantification. *Nature Biotechnology.* 2016;34(5):525-7.

770 47. Grande BM, Gerhard DS, Jiang A, Griner NB, Abramson JS, Alexander TB, et al. Genome-  
771 wide discovery of somatic coding and noncoding mutations in pediatric endemic and sporadic  
772 Burkitt lymphoma. *Blood.* 2019;133(12):1313-24.

773 48. Cristescu R, Lee J, Nebozhyn M, Kim K-M, Ting JC, Wong SS, et al. Molecular analysis of  
774 gastric cancer identifies subtypes associated with distinct clinical outcomes. *Nature Medicine.*  
775 2015;21(5):449-56.

776 49. Love MI, Huber W, Anders S. Moderated estimation of fold change and dispersion for  
777 RNA-seq data with DESeq2. *Genome Biology*. 2014;15(12).

778 50. Huber W, Von Heydebreck A, Sultmann H, Poustka A, Vingron M. Variance stabilization  
779 applied to microarray data calibration and to the quantification of differential expression.  
780 *Bioinformatics*. 2002;18(Suppl 1):S96-S104.

781 51. McFadden D. Conditional logic analysis of qualitative choice behavior. [Berkeley]: [Institute  
782 of Urban & Regional Development, University of California]; 1972.

783 52. Szklarczyk D, Gable AL, Lyon D, Junge A, Wyder S, Huerta-Cepas J, et al. STRING v11:  
784 protein–protein association networks with increased coverage, supporting functional discovery in  
785 genome-wide experimental datasets. *Nucleic Acids Research*. 2019;47(D1):D607-D13.

786 53. Kuleshov MV, Jones MR, Rouillard AD, Fernandez NF, Duan Q, Wang Z, et al. Enrichr: a  
787 comprehensive gene set enrichment analysis web server 2016 update. *Nucleic Acids Research*.  
788 2016;44(W1):W90-W7.

789 54. Dalla-Favera R, Bregni M, Erikson J, Patterson D, Gallo RC, Croce CM. Human c-myc onc  
790 gene is located on the region of chromosome 8 that is translocated in Burkitt lymphoma cells.  
791 *Proceedings of the National Academy of Sciences*. 1982;79(24):7824-7.

792 55. Neel BG, Jhanwar SC, Chaganti RS, Hayward WS. Two human c-onc genes are located  
793 on the long arm of chromosome 8. 1982;79(24):7842-6.

794 56. TCGA. Comprehensive molecular characterization of gastric adenocarcinoma. *Nature*.  
795 2014;513(7517):202-9.

796 57. Van Cutsem E, Sagaert X, Topal B, Haustermans K, Prenen H. Gastric cancer. *The  
797 Lancet*. 2016;388(10060):2654-64.

798 58. Cancer Genome Atlas Research N. Comprehensive molecular characterization of gastric  
799 adenocarcinoma. *Nature*. 2014;513(7517):202-9.

800 59. Brown BD, Gentner B, Cantore A, Colleoni S, Amendola M, Zingale A, et al. Endogenous  
801 microRNA can be broadly exploited to regulate transgene expression according to tissue, lineage  
802 and differentiation state. 2007;25(12):1457-67.

803 60. Ma L, Teruya-Feldstein J, Weinberg RA. Tumour invasion and metastasis initiated by  
804 microRNA-10b in breast cancer. *Nature*. 2007;449(7163):682-8.

805 61. Flores O, Kennedy EM, Skalsky RL, Cullen BR. Differential RISC association of  
806 endogenous human microRNAs predicts their inhibitory potential. *Nucleic acids research*.  
807 2014;42(7):4629-39.

808 62. Helwak A, Kudla G, Dudnakova T, Tollervey D. Mapping the Human miRNA Interactome  
809 by CLASH Reveals Frequent Noncanonical Binding. *Cell*. 2013;153(3):654-65.

810 63. Yang YC, Liem A, Lambert PF, Sugden B. Dissecting the regulation of EBV's BART  
811 miRNAs in carcinomas. *Virology*. 2017;505:148-54.

812 64. Qiu J, Smith P, Leahy L, Thorley-Lawson DA. The Epstein-Barr virus encoded BART  
813 miRNAs potentiate tumor growth in vivo. *PLoS Pathog*. 2015;11(1):e1004561.

814 65. Bullard WL, Kara M, Gay LA, Sethuraman S, Wang Y, Nirmalan S, et al. Identification of  
815 murine gammaherpesvirus 68 miRNA-mRNA hybrids reveals miRNA target conservation among  
816 gammaherpesviruses including host translation and protein modification machinery. *PLOS*  
817 *Pathogens*. 2019;15(8):e1007843.

818 66. Feldman ER, Kara M, Oko LM, Grau KR, Krueger BJ, Zhang J, et al. A Gammaherpesvirus  
819 Noncoding RNA Is Essential for Hematogenous Dissemination and Establishment of Peripheral  
820 Latency. *mSphere*. 2016;1(2).

821 67. Arvey A, Larsson E, Sander C, Leslie CS, Marks DS. Target mRNA abundance dilutes  
822 microRNA and siRNA activity. 2010;6.

823 68. Schirle NT, Sheu-Gruttaduria J, Macrae IJ. Structural basis for microRNA targeting.  
824 *Science*. 2014;346(6209):608-13.

825 69. McGeary SE, Lin KS, Shi CY, Pham TM, Bisaria N, Kelley GM, et al. The biochemical  
826 basis of microRNA targeting efficacy. *Science*. 2019;366(6472):eaav1741.

827 70. Ameres SL, Martinez J, Schroeder R. Molecular Basis for Target RNA Recognition and  
828 Cleavage by Human RISC. *Cell*. 2007;130(1):101-12.

829 71. Bernhart SH, Hofacker IL, Stadler PF. Local RNA base pairing probabilities in large  
830 sequences. *Bioinformatics*. 2006;22(5):614-5.

831 72. Garcia DM, Baek D, Shin C, Bell GW, Grimson A, Bartel DP. Weak seed-pairing stability  
832 and high target-site abundance decrease the proficiency of lsy-6 and other microRNAs. *Nature*  
833 *Structural & Molecular Biology*. 2011;18(10):1139-46.

834 73. Strong MJ, Xu G, Coco J, Baribault C, Vinay DS, Lacey MR, et al. Differences in gastric  
835 carcinoma microenvironment stratify according to EBV infection intensity: implications for possible  
836 immune adjuvant therapy. *PLoS Pathog*. 2013;9(5):e1003341.

837 74. Newman AM, Steen CB, Liu CL, Gentles AJ, Chaudhuri AA, Scherer F, et al. Determining  
838 cell type abundance and expression from bulk tissues with digital cytometry. *Nature*  
839 *Biotechnology*. 2019;37(7):773-82.

840 75. Bolotin DA, Poslavsky S, Mitrophanov I, Shugay M, Mamedov IZ, Putintseva EV, et al.  
841 MiXCR: software for comprehensive adaptive immunity profiling. *Nature Methods*.  
842 2015;12(5):380-1.

843 76. Shugay M, Bagaev DV, Turchaninova MA, Bolotin DA, Britanova OV, Putintseva EV, et al.  
844 VDJtools: Unifying Post-analysis of T Cell Receptor Repertoires. *PLOS Computational Biology*.  
845 2015;11(11):e1004503.

846 77. Mootha VK, Lindgren CM, Eriksson K-F, Subramanian A, Sihag S, Lehar J, et al. PGC-1 $\alpha$ -  
847 responsive genes involved in oxidative phosphorylation are coordinately downregulated in human  
848 diabetes. *Nature Genetics*. 2003;34(3):267-73.

849 78. Subramanian A, Tamayo P, Mootha VK, Mukherjee S, Ebert BL, Gillette MA, et al. Gene  
850 set enrichment analysis: a knowledge-based approach for interpreting genome-wide expression  
851 profiles. *Proc Natl Acad Sci U S A*. 2005;102(43):15545-50.

852 79. Farh KKH. The Widespread Impact of Mammalian MicroRNAs on mRNA Repression and  
853 Evolution. *Science*. 2005;310(5755):1817-21.

854 80. Simkin A, Geissler R, McIntyre ABR, Grimson A. Evolutionary dynamics of microRNA  
855 target sites across vertebrate evolution. *PLOS Genetics*. 2020;16(2):e1008285.

856 81. Agarwal V, Bell GW, Nam J-W, Bartel DP. Predicting effective microRNA target sites in  
857 mammalian mRNAs. *eLife*. 2015;4.

858 82. Hafner M, Landthaler M, Burger L, Khorshid M, Hausser J, Berninger P, et al.  
859 Transcriptome-wide identification of RNA-binding protein and microRNA target sites by PAR-  
860 CLIP. *Cell*. 2010;141(1):129-41.

861 83. Mishra R, Kumar A, Ingle H, Kumar H. The Interplay Between Viral-Derived miRNAs and  
862 Host Immunity During Infection. *Frontiers in Immunology*. 2020;10.

863 84. Choy EY-W, Siu K-L, Kok K-H, Lung RW-M, Tsang CM, To K-F, et al. An Epstein-Barr  
864 virus-encoded microRNA targets PUMA to promote host cell survival. 2008;205(11):2551-60.

865 85. Kim H, Choi H, Lee SK. Epstein-Barr Virus MicroRNA miR-BART20-5p Suppresses Lytic  
866 Induction by Inhibiting BAD -Mediated caspase-3 -Dependent Apoptosis. 2016;90(3):1359-68.

867 86. Kanda T, Miyata M, Kano M, Kondo S, Yoshizaki T, Iizasa H. Clustered MicroRNAs of the  
868 Epstein-Barr Virus Cooperatively Downregulate an Epithelial Cell-Specific Metastasis  
869 Suppressor. *Journal of Virology*. 2015;89(5):2684-97.

870 87. Nachmani D, Stern-Ginossar N, Sarid R, Mandelboim O. Diverse herpesvirus microRNAs  
871 target the stress-induced immune ligand MICB to escape recognition by natural killer cells. *Cell*  
872 *Host Microbe*. 2009;5(4):376-85.

873 88. Tagawa T, Albanese M, Bouvet M, Moosmann A, Mautner J, Heissmeyer V, et al. Epstein-  
874 Barr viral miRNAs inhibit antiviral CD4+ T cell responses targeting IL-12 and peptide processing.  
875 The Journal of Experimental Medicine. 2016;213(10):2065-80.

876 89. Klinke O, Feederle R, Delecluse H-J. Genetics of Epstein–Barr virus microRNAs. Seminars  
877 in Cancer Biology. 2014;26:52-9.

878 90. Dolken L, Malterer G, Erhard F, Kothe S, Friedel CC, Suffert G, et al. Systematic analysis  
879 of viral and cellular microRNA targets in cells latently infected with human gamma-herpesviruses  
880 by RISC immunoprecipitation assay. Cell Host Microbe. 2010;7(4):324-34.

881 91. Yu Z, Chen T, Li X, Yang M, Tang S, Zhu X, et al. Lys29-linkage of ASK1 by Skp1–Cullin  
882 1–Fbxo21 ubiquitin ligase complex is required for antiviral innate response. eLife. 2016;5.

883 92. Lang X, Tang T, Jin T, Ding C, Zhou R, Jiang W. TRIM65-catalized ubiquitination is  
884 essential for MDA5-mediated antiviral innate immunity. The Journal of Experimental Medicine.  
885 2017;214(2):459-73.

886 93. Li Q, Yan J, Mao AP, Li C, Ran Y, Shu HB, et al. Tripartite motif 8 (TRIM8) modulates  
887 TNF - and IL-1 -triggered NF- B activation by targeting TAK1 for K63-linked polyubiquitination.  
888 Proceedings of the National Academy of Sciences. 2011;108(48):19341-6.

889 94. Albanese M, Tagawa T, Bouvet M, Maliqi L, Lutter D, Hoser J, et al. Epstein–Barr virus  
890 microRNAs reduce immune surveillance by virus-specific CD8+T cells. Proceedings of the  
891 National Academy of Sciences. 2016;113(42):E6467-E75.

892 95. Murer A, Rühl J, Zbinden A, Capaul R, Hammerschmidt W, Chijioke O, et al. MicroRNAs of  
893 Epstein-Barr Virus Attenuate T-Cell-Mediated Immune Control In Vivo. mBio. 2019;10(1).

894 96. Le Gall S, Erdtmann L, Benichou S, Berlioz-Torrent C, Liu L, Benarous R, et al. Nef  
895 interacts with the mu subunit of clathrin adaptor complexes and reveals a cryptic sorting signal in  
896 MHC I molecules. Immunity. 1998;8(4):483-95.

897 97. Hu Z, Zhang Z, Doo E, Coux O, Goldberg AL, Liang TJ. Hepatitis B virus X protein is both  
898 a substrate and a potential inhibitor of the proteasome complex. *J Virol.* 1999;73(9):7231-40.

899 98. Coscoy L, Ganem D. Kaposi's sarcoma-associated herpesvirus encodes two proteins that  
900 block cell surface display of MHC class I chains by enhancing their endocytosis. *Proceedings of*  
901 *the National Academy of Sciences.* 2000;97(14):8051-6.

902 99. Boname JM, Stevenson PG. MHC Class I Ubiquitination by a Viral PHD/LAP Finger  
903 Protein. *Immunity.* 2001;15(4):627-36.

904 100. Ahn K, Gruhler A, Galocha B, Jones TR, Wiertz EJHJ, Ploegh HL, et al. The ER-Luminal  
905 Domain of the HCMV Glycoprotein US6 Inhibits Peptide Translocation by TAP. *Immunity.*  
906 1997;6(5):613-21.

907 101. Horst D, Van Leeuwen D, Croft NP, Garstka MA, Hislop AD, Kremmer E, et al. Specific  
908 Targeting of the EBV Lytic Phase Protein BNLF2a to the Transporter Associated with Antigen  
909 Processing Results in Impairment of HLA Class I-Restricted Antigen Presentation. *The Journal of*  
910 *Immunology.* 2009;182(4):2313-24.

911 102. Raftery MJ, Schwab M, Eibert SM, Samstag Y, Walczak H, Schönrich G. Targeting the  
912 Function of Mature Dendritic Cells by Human Cytomegalovirus. 2001;15(6):997-1009.

913 103. McGranahan N, Furness AJS, Rosenthal R, Ramskov S, Lyngaa R, Saini SK, et al. Clonal  
914 neoantigens elicit T cell immunoreactivity and sensitivity to immune checkpoint blockade.  
915 *Science.* 2016;351(6280):1463-9.

916 104. Yang Y-C, Liem A, Lambert PF, Sugden B. Dissecting the regulation of EBV's BART  
917 miRNAs in carcinomas. 2017;505:148-54.

918 105. O'Grady T, Cao S, Strong MJ, Concha M, Wang X, Splinter Bondurant S, et al. Global  
919 bidirectional transcription of the Epstein-Barr virus genome during reactivation. *J Virol.*  
920 2014;88(3):1604-16.

921 106. Grande BM, Gerhard DS, Jiang A, Griner NB, Abramson JS, Alexander TB, et al. Genome-  
922 wide discovery of somatic coding and noncoding mutations in pediatric endemic and sporadic  
923 Burkitt lymphoma. *Blood*. 2019;133(12):1313-24.

924 107. Ungerleider N, Flemington E. SpliceV: analysis and publication quality printing of linear and  
925 circular RNA splicing, expression and regulation. *BMC Bioinformatics*. 2019;20(1):231.

926 108. Lorenz R, Bernhart SH, Höner Zu Siederdissen C, Tafer H, Flamm C, Stadler PF, et al.  
927 ViennaRNA Package 2.0. *Algorithms for Molecular Biology*. 2011;6(1):26.

928 109. Grimson A, Farh KK-H, Johnston WK, Garrett-Engele P, Lim LP, Bartel DP. MicroRNA  
929 Targeting Specificity in Mammals: Determinants beyond Seed Pairing. *Molecular Cell*.  
930 2007;27(1):91-105.

931